Dioxomolybdenum(VI) Complexes of Tripodal Nitrogen-Donor Ligands: Syntheses and Spectroscopic, Structural, and Electrochemical Studies, Including the Generation of EPR-Active Molybdenum(V) Species in Solution

Zhiguang Xiao,[†] Michael A. Bruck,[‡] Colleen Doyle,[‡] John H. Enemark,*[,‡] Carina Grittini,[‡] Robert W. Gable,[†] Anthony G. Wedd,[†] and Charles G. Young[†]

School of Chemistry, University of Melbourne, Parkville, Victoria 3052, Australia, and Department of Chemistry, University of Arizona, Tucson, Arizona 85721

Received April 6, 1995[⊗]

The dioxo–Mo(VI) complexes $LMoO_2X$ [L = hydrotris(3,5-dimethylpyrazol-1-yl)borate (L^a), hydrotris(3-isopropylpyrazol-1-yl)borate (L^b), hydrotris(3,5-dimethyl-1,2,4-triazol-1-yl)borate (L^c); X = Cl, Br, NCS, OMe, OEt, OPh, SPr^i, SPh, SCH_2Ph] have been synthesized and characterized by spectroscopic and structural methods. The infrared spectra of the complexes exhibit $\nu(MoO_2)$ bands at 940–920 and 910–890 cm^{-1}, and the ^1H NMR spectra are indicative of molecular C_s symmetry in solution. The X-ray crystal structures of three complexes are reported. $L^aMoO_2(SPh)$: monoclinic space group $P2_1/c$, a = 18.265(6) Å, b = 8.110(3) Å, c = 18.299(3) Å, β = 117.06(2)°, V = 2414(1) $Å^3$ with Z = 4. $L^bMoO_2(OMe)$: monoclinic space group $C2/c$, a = 30.365(4) Å, b = 8.373(1) Å, c = 19.646(2) Å, β = 113.28(1)°, V = 4588(1) $Å^3$ with Z = 8. $L^cMoO_2(SPh)$: orthorhombic space group $P2_12_12_1$, a = 7.9302(13) Å, b = 16.627(2) Å, c = 17.543(2) Å, V = 2313.1(9) $Å^3$ with Z = 4. The structures were refined by full-matrix least-squares procedures to R values of 0.043, 0.027, and 0.039, respectively. The mononuclear complexes feature facially tridentate N-donor ligands, mutually *cis* oxo and X ligands, and distorted octahedral geometries. The alkoxy and thiolate complexes undergo a reversible, one-electron reduction to form the corresponding dioxo–Mo(V) anions $[LMo^VO_2X]^-$. The requirements for *reversible*, one-electron electrochemical reduction of dioxo–Mo(VI) complexes appear to be (i) minimal conformational change, restricting substitution *trans* to the oxo groups, upon reduction and (ii) a steric or electrostatic barrier to the close approach and dinucleation of the reduced species. A number of oxo–hydroxo–Mo(V) complexes of the type $LMo^VO(OH)X$ were generated by protonation of the anions $[LMo^VO_2X]^-$. Chemical reduction by Bu^n_4NSH results in the sequential generation of $[LMo^VO_2X]^-$ and $[LMo^VOSX]^-$ anions (except for X = OPh, SPh, and SPr^i, when only $[LMo^VO_2X]^-$ is formed). The Mo(V) complexes have been characterized by EPR spectroscopy.

Introduction

Tris(pyrazolyl)borate and related tripodal N-donor ligands[1] have had a significant impact on the modeling of molybdenum,[2–5] copper,[6] and zinc[7] enzymes. These ligands occupy a single face of a pseudo-octahedral or -tetrahedral metal site and control access to the coligand position(s) according to the nature and pattern of the pyrazole ring substituents. Substitution at the 3-positions effectively inhibits polynucleation of molybdenum complexes, and for this reason the hydrotris(3,5-dimethylpyrazol-1-yl)borate ligand (L^a)[8] has played an important role in the modeling of mononuclear molybdenum enzyme sites.[2–5] Work with this ligand has produced a variety of Mo(VI),[9–11] Mo(V),[11–16] and Mo(IV)[9–11,17] complexes which model various facets of enzyme structure, spectroscopy, and reactivity. Steric and electronic fine-tuning, achieved through the systematic variation of coligands, has produced a catalytic system which combines oxygen atom transfer[18] and coupled electron–proton

* Author to whom correspondence should be addressed.
† University of Melbourne.
‡ University of Arizona.
⊗ Abstract published in *Advance ACS Abstracts,* November 1, 1995.

(1) (a) Trofimenko, S. *Chem. Rev.* **1972**, *72*, 497. (b) Trofimenko, S. *Prog. Inorg. Chem.* **1986**, *34*, 115. (c) Trofimenko, S. *Chem. Rev.* **1993**, *93*, 943.
(2) (a) *Molybdenum Enzymes, Cofactors, and Model Systems*; Stiefel, E. I., Coucouvanis, D., Newton, W. E., Eds.; ACS Symposium Series 535; American Chemical Society: Washington, DC, 1993. (b) Young, C. G.; Wedd, A. G. In ref 2a, p 70.
(3) Enemark, J. H.; Young, C. G. *Adv. Inorg. Chem.* **1993**, *40*, 1 and references therein.
(4) Young, C. G.; Wedd, A. G. *Encyclopedia of Inorganic Chemistry*; King, R. B., Ed.; Wiley: New York, 1994; p 2330 and references therein.
(5) Pilato, R. S.; Stiefel, E. I. In *Inorganic Catalysis*; Reedijk, J., Ed.; Marcel Dekker: New York, 1993; p 131.
(6) Kitajima, N.; Moro-oka, Y. *Chem. Rev.* **1994**, *94*, 737.
(7) (a) Ruf, M.; Weis, K.; Vahrenkamp, H. *J. Chem. Soc., Chem. Commun.* **1994**, 135. (b) Looney, A.; Han, R.; McNeill, K.; Parkin, G. *J. Am. Chem. Soc.* **1993**, *115*, 4690. (c) Looney, A.; Parkin, G.; Alsfasser, R.; Ruf, M.; Vahrenkamp, H. *Angew. Chem., Int. Ed. Engl.* **1992**, *31*, 92.
(8) Abbreviations: L = L^a, L^b, L^c; L^a = hydrotris(3,5-dimethylpyrazol-1-yl)borate, L^b = hydrotris(3-isopropylpyrazol-1-yl)borate, L^c = hydrotris(3,5-dimethyl-1,2,4-triazol-1-yl)borate. $L{-}N_2S_2$ = dianion of *N,N'*-dimethyl-*N,N'*-bis(2-mercaptophenyl)-1,2-diaminoethane. THF = tetrahydrofuran.
(9) Roberts, S. A.; Young, C. G.; Cleland, W. E., Jr.; Ortega, R. B.; Enemark, J. H. *Inorg. Chem.* **1988**, *27*, 3044.
(10) Roberts, S. A.; Young, C. G.; Kipke, C. A.; Cleland, W. E., Jr.; Yamanouchi, K.; Carducci, M. D.; Enemark, J. H. *Inorg. Chem.* **1990**, *29*, 3650.
(11) Xiao, Z.; Young, C. G.; Enemark, J. H.; Wedd, A. G. *J. Am. Chem. Soc.* **1992**, *114*, 9194.
(12) Cleland, W. E., Jr.; Barnhart, K. M.; Yamanouchi, K.; Collison, D.; Mabbs, F. E.; Ortega, R. B.; Enemark, J. H. *Inorg. Chem.* **1987**, *26*, 1017.
(13) Young, C. G.; Enemark, J. H.; Collison, D.; Mabbs, F. E. *Inorg. Chem.* **1987**, *26*, 2925.
(14) (a) Chang, C.-S. J.; Collison, D.; Mabbs, F. E.; Enemark, J. H. *Inorg. Chem.* **1990**, *29*, 2261. (b) Chang, C.-S. J.; Enemark, J. H. *Inorg. Chem.* **1991**, *30*, 683.
(15) Basu, P.; Raitsimring, A. M.; LaBarre, M. J.; Dhawan, I. K.; Weibrecht, J. L.; Enemark, J. H. *J. Am. Chem. Soc.* **1994**, *116*, 7166.
(16) Dhawan, I. K.; Pacheco, A.; Enemark, J. H. *J. Am. Chem. Soc.* **1994**, *116*, 7911.
(17) Young, C. G.; Roberts, S. A.; Ortega, R. B.; Enemark, J. H. *J. Am. Chem. Soc.* **1987**, *109*, 2938.

0020-1669/95/1334-5950$09.00/0

Table 1. Infrared Data for $LMoO_2X$ Complexes (cm^{-1})[a]

	$\nu(MoO_2)$			$\nu(Mo-X)$			$\nu(B-H)$		
X	L^a	L^b	L^c	L^a	L^b	L^c	L^a	L^b	L^c
Cl	930 s	939 s	938 s	349 m	341 m		2548 m	2508 m	2545 m
	900 s	906 s	910 s						
Br	929 s	938 s	938 s				2550 m	2504 m	2545 m
	899 s	905 s	908 s						
OMe	922 s	924 s	930 s	536 m	544 s	539 s	2549 m	2495 m	2545 m
	900 s	903 s	905 s						
OEt	925 s	932 s		586 m	616 m		2546 m	2507 m	
	897 s	902 s							
OPr^n	922 s						2547 m		
	897 s								
OPh	924 s	931 s	934 s				2545 m	2498 m	2545 m
	897 s	900 s	906 s						
SPh	922 s	924 s	930 s	427 m	493 w	428 w	2539 m	2515 m	2556 m
	890 s	897 s	900 s						
SPr^i	923 s		926 s	436 m		437 w	2544 m		2554 m
	891 s		895 s						
SCH_2Ph	920 s		927 s	565 m		556 w	2544 m		2554 m
	890 s		897 s						

[a] As KBr disks; w = weak, m = medium, s = strong intensity.

transfer reactions[19] (cf. sulfite oxidase and related enzymes) and permits the generation of Mo(V) complexes such as $[LMo^VO_2(SPh)]^-$ and $L^aMoO^V(OH)(SPh)$.[11,20] The choice of coligand was crucial also to the stabilization of the oxo–thio–Mo(VI) complex $L^aMoOS(S_2PPr^i_2)$, the first valid model of the oxidized active form of xanthine oxidase.[21] To a significant extent, the refinement of these systems is dependent on synthetic access to dioxo–Mo(VI) complexes of the type $LMoO_2X$ and the systematic study of their behavior through variation of L and X.

This paper reports improved syntheses for some known L^aMoO_2X complexes and the adaption of these syntheses to the task of extending the range of coligands X. New complexes containing hydrotris(3-isopropylpyrazol-1-yl)borate (L^b) and hydrotris(3,5-dimethyl-1,2,4-triazol-1-yl)borate (L^c) are described also. As well, we report the generation of EPR-active Mo(V) complexes such as $[LMo^VO_2X]^-$, $LMo^VO(OH)X$, and $[LMo^VOSX]^-$ by a variety of electrochemical and chemical processes. This aspect of our work complements previous studies of related $[(L\text{-}N_2S_2)Mo^VO_2]^-$, $[(L\text{-}N_2S_2)Mo^VOS]^-$, and $(L\text{-}N_2S_2)Mo^VO(EH)$ complexes (E = O, S).[8,22–24] The paper focuses on the Mo(VI) component of a broad functional model for the pterin-containing molybdenum enzymes[11] and selected Mo(V) solution chemistry.

Experimental Section

Ligands. The method of Trofimenko[25] was employed in the synthesis of KL^a. A modification of the literature method was employed in the synthesis of KL^b.[26] A free-flowing powder was isolated in 55% yield by addition of *dry* hexane, rather than tetrahydrofuran, with vigorous stirring to the reaction residue after excess 3-isopropylpyrazole had been distilled away. ^1H NMR ($CDCl_3$): δ 1.05 (d, 18H, 6 CH_3), 2.74 (septet, 3H, 3 CH), 5.93 (d, 3H, 3 CH), *ca.* 6.9 (broad, 3H, 3 CH).

Samples of KL^c were prepared by gradually heating a finely ground mixture of 3,5-dimethyl-1,2,4-triazole[27] (50 g, 0.51 mol) and KBH_4 (6.0 g, 0.11 mol) to *ca.* 140 °C, whereupon melting and rapid evolution of H_2 gas took place. Heating was continued with evolution of 2 and then 3 equiv of H_2 (at *ca.* 170 and 200 °C, respectively). The partly-solidified melt was heated at 230–250 °C for another 2 h before being cooled to room temperature and finely ground. Excess triazole was removed by sublimation at 130 °C under vacuum. Yield: 35.7 g (96%). IR (KBr): 2925 m, ν(BH) 2500 m, 1510 s, 1490 s, 1410, s, br, 1375 w, 1370 w, 1335 s, 1220 s, 1195 m, 1075 s, 1040 m, 1005 m, 980 m, 950 m, 820 s, 710 s, 700 s, 670 s, 620 w, 475 w cm^{-1}. ^1H NMR (D_2O): δ 1.90 (s, 9H, 3 CH_3), 2.05 (s, 9H, 3 CH_3).

Complexes $LMoO_2X$. Unless specified, all reactions were carried out under an atmosphere of purified dinitrogen using standard Schlenk line techniques and dried, deoxygenated solvents. Workups were generally performed in air without special precautions. Microanalyses were performed (on representative compounds only) by Atlantic Microlabs, Norcross, GA. Infrared and ^1H NMR data are given in Tables 1 and 2, respectively.

$LMoO_2Cl$. These complexes were prepared from $MoO_2Cl_2(OPPh_3)_2$[28] by adaption of the literature method.[10] For L^bMoO_2Cl and L^cMoO_2Cl, the reaction mixtures were concentrated to a small volume before addition of methanol as precipitant. The crude products were recrystallized from CH_2Cl_2/MeOH.

L^bMoO_2Cl: Yield 58%. Anal. Calcd for $C_{18}H_{28}BClMoN_6O_2$: C, 43.01; H, 5.61; N, 16.72; Cl, 7.05. Found: C, 42.93; H, 5.62; N, 16.85; Cl, 7.22.

L^cMoO_2Cl: Yield 56%. Anal. Calcd for $C_{12}H_{19}BClMoN_6O_2$: C, 31.10; H, 4.13; N, 27.20; Cl, 7.65. Found: C, 31.05; H, 4.05; N, 27.40; Cl, 7.60.

$LMoO_2Br$. These complexes were prepared from $MoO_2Br_2(Me_2SO)_2$[29] by adaption of the literature method.[10] The L^aMoO_2Br complex needed to be further purified by column chromatography on silica gel (CH_2Cl_2) to remove contaminants, particularly $[L^aMoO_2]_2(\mu\text{-}O)$.[30] This was not necessary in the synthesis of L^bMoO_2Br, which was precipitated using methanol and recrystallized from CH_2Cl_2/MeOH. Crude L^cMoO_2Br, isolated by filtration from the partially concentrated reaction mixture, was purified by Soxhlet extraction with CH_2Cl_2 and recrystallized from CH_2Cl_2/hexane.

(18) Holm, R. H. *Chem. Rev.* **1987**, *87*, 1401.
(19) Stiefel, E. I. *Proc. Natl. Acad. Sci. U.S.A.* **1973**, *70*, 988.
(20) (a) Xiao, Z.; Gable, R. W.; Wedd, A. G.; Young, C. G. *J. Chem. Soc., Chem. Commun.* **1994**, 1295. (b) Xiao, Z.; Gable, R. W.; Wedd, A. G.; Young, C. G. Submitted for publication.
(21) Eagle, A. A.; Laughlin, L. J.; Young, C. G.; Tiekink, E. R. T. *J. Am. Chem. Soc.* **1992**, *114*, 9195.
(22) Dowerah, D.; Spence, J. T.; Singh, R.; Wedd, A. G.; Wilson, G. L.; Farchione, F.; Enemark, J. H.; Kristofzski, J.; Bruck, M. *J. Am. Chem. Soc.* **1987**, *109*, 5655.
(23) Wilson, G. L.; Greenwood, R. J.; Pilbrow, J. R.; Spence, J. T.; Wedd, A. G. *J. Am. Chem. Soc.* **1991**, *113*, 6803.
(24) Greenwood, R. J.; Wilson, G. L.; Pilbrow, J. R.; Wedd, A. G. *J. Am. Chem. Soc.* **1993**, *115*, 5385.
(25) Trofimenko, S. *J. Am. Chem. Soc.* **1967**, *89*, 6288.
(26) Trofimenko, S.; Calabrese, J. C.; Domaille, P. J.; Thompson, J. S. *Inorg. Chem.* **1989**, *28*, 1091.
(27) Jones, R. L.; Rees, C. W. *J. Chem. Soc. C* **1969**, 2251.
(28) Butcher, R. J.; Penfold, B. R.; Sinn, E. *J. Chem. Soc., Dalton Trans.* **1979**, 668.
(29) Butcher, R. J.; Gunz, H. P.; Maclagan, R. G. A. R.; Powell, H. K. J.; Wilkins, C. J.; Hian, Y. S. *J. Chem. Soc., Dalton Trans.* **1975**, 1223.
(30) Xiao, Z.; Enemark, J. H.; Wedd, A. G.; Young C. G. *Inorg. Chem.* **1994**, *33*, 3438.

Table 2. ^{1}H NMR Data

(a) $L^{a,c}MoO_2X$ Complexes in $CDCl_3$

L	X	L ligand[a] CH_3 (each 6H)	L ligand[a] CH_3 (each 3H)	L ligand[a] 4-C*H* (2H)	L ligand[a] 4-C*H* (1H)	X ligand[b,c]
L^a	Cl	2.36, 2.65	2.34, 2.61	5.84	5.83	
	Br	2.36, 2.70	2.33, 2.58	5.85	5.83	
	NCS	2.36, 2.60	2.35, 2.57	5.85	5.86	
	OMe	2.33, 2.55	2.32, 2.74	5.80	5.82	4.24 s
	OEt	2.32, 2.54	2.32, 2.73	5.78	5.81	1.41 t (7.0); 4.62 q (7.0)
	OPr^n	2.33, 2.54	2.31, 2.73	5.79	5.80	0.94 t (7.3); 1.80 h (7.3); 4.47 t (7.2)
	OPh	2.31, 2.38	2.37, 2.79	5.78	5.87	6.90−7.27 m
	SPh	2.38, 2.71	2.35, 2.61	5.85	5.85	7.10 t (7.4); 7.30 t (7.5); 7.68 d (7.4)
	SPr^i	2.34, 2.74	2.32, 2.61	5.81	5.80	1.55 d (6.8); 3.86 m
	SCH_2Ph[d]	2.35, 2.68	2.33, 2.55	5.85	5.86	4.41 s; 7.14−7.36 m
L^c	Cl	2.55, 2.76	2.54, 2.76			
	Br	2.55, 2.81	2.53, 2.73			
	OMe	2.51, 2.65	2.50, 2.83			4.38 s
	OPh	2.42, 2.56	2.56, 2.90			6.94 d (7.8); 7.01 t (7.3); 7.30 t (7.9)
	SPh	2.56, 2.83	2.53, 2.72			7.16 t (7.3); 7.34 t (7.7); 7.61 d (8.0)
	SPr^i	2.53, 2.83	2.51, 2.74			1.56 d (6.6); 3.93 m
	SCH_2Ph	2.53, 2.77	2.52, 2.73			4.64 s; 7.23−7.42 m

(b) L^bMoO_2X in $CDCl_3$

X	L^b ligand[b] CH_3 (each 6H)[e]	L^b ligand[b] $-CHMe_2$[f]	L^b ligand[b] 4-C*H*[e,g]	L^b ligand[b] 5-C*H*[e,g]	X ligand[b,c]
Cl	1.20 (6.7)	4.02 m (3H)	6.12 (2.4)	7.58 (2.4)	
	1.20 (6.7)		6.10 (2.4)	7.60 (2.4)	
	1.26 (7.0)				
Br	1.19 (6.7)	4.14 (6.7)	6.12 (2.1)	7.59 (1.8)	
	1.19 (6.7)	3.97 (6.7)	6.08(2.1)	7.59 (1.8)	
	1.28 (6.7)				
OMe	1.20−1.27	3.74 (6.9)	6.07 (2.1)	7.53−7.56	4.22 s
	(5 peaks)	4.31 (6.9)	6.07 (2.1)	(3 peaks)	
OEt	1.19−1.25	3.75 (6.7)	6.06 (1.8)	7.53 (1.8)	1.39 t (7.0)
	(3 peaks)	4.31 (6.7)	6.06 (1.8)	7.53 (1.8)	4.59 q (7.0)
OPh	0.92 (6.7)	3.45 (6.8)	6.06 (2.1)	7.59 (2.1)	6.81 d (8.2)
	1.08 (6.7)	4.37 (6.7)	6.13 (2.4)	7.61 (2.4)	6.91 t (7.3)
	1.27 (6.7)				7.22 t (7.9)
SPh	1.11−1.29	4.16 (6.7)	6.12 (2.1)	7.60−7.66	7.12−7.50 m
	(6 peaks)	3.98 (6.7)	6.08 (1.8)	(4 peaks)	

[a] All singlets. [b] *J* (Hz) given in parentheses. [c] s = singlet, d = doublet, t = triplet, q = quartet, m = multiplet. [d] In CD_2Cl_2. [e] Unless specified, all doublets. [f] All septets, 2H and 1H integration, respectively. [g] Integration: 2H and 1H, respectively.

L^bMoO_2Br: Yield 30%.

L^cMoO_2Br: Yield 45%. Anal. Calcd for $C_{12}H_{19}BBrN_9MoO_2$: C, 28.37; H, 3.77; N, 24.81; Br, 15.73. Found: C, 28.21; H, 3.76; N, 24.67; Br, 15.88.

$L^aMoO_2(OR)$ (R = Me, Et, Pr^n). To a yellow suspension of L^aMoO_2Br (0.55 g, 1.1 mmol) in CH_2Cl_2 (20 mL) was added saturated NaOH/ROH solution (2.0 mL). The reaction mixture was stirred at 40−50 °C in air for 10, 30, and 60 min for R = Me, Et, and Pr^n, respectively, and then evaporated to dryness under vacuum. The white residue was dissolved in CH_2Cl_2, and insoluble materials (NaBr and NaOH) were removed by filtration. Addition of methanol to the concentrated filtrate produced a white solid. Yields were 80−86%.

$L^bMoO_2(OR)$ (R = Me, Et). To a pale-yellow solution of L^bMoO_2Cl (0.3 g, 0.6 mmol) in CH_2Cl_2 (15 mL) was added saturated NaOH/ROH solution (1.0 mL). After being stirred for 20 min at room temperature, the solution was evaporated to dryness. The white residue was redissolved in CH_2Cl_2 and insoluble material filtered off. The white product was recrystallized from CH_2Cl_2/MeOH. Yields were 67% for $L^bMoO_2(OMe)$ and 50% for $L^bMoO_2(OEt)$.

$L^cMoO_2(OMe)$. A pale-yellow solution of L^cMoO_2Br (0.51 g, 1.0 mmol) in a mixed solvent of MeOH/CH_2Cl_2 (10/10 mL) turned colorless slowly upon being stirred at room temperature for *ca.* 6 h. The solution was evaporated to dryness under vacuum. The white residue was redissolved in CH_2Cl_2 and insoluble material filtered off. The white product was obtained by removing the solvent under vacuum. Yield: 0.42 g (92%).

$LMoO_2(OPh)$. Orange $L^aMoO_2(OPh)$ was prepared by a modification of the literature method.[10] To a mixture of L^aMoO_2Br (2.0 g, 4.0 mmol) and phenol (1.5 g, 16 mmol) was added dichloroethane (40 mL) and triethylamine (2.0 mL, 15 mmol). After being stirred at 70 °C for 5 h, the solution was concentrated to small volume and chromatographed on a silica gel column using toluene as eluant. The first orange band was collected and the product recrystallized from CH_2Cl_2/MeOH. Yield: 1.6 g (78%). The orange $L^bMoO_2(OPh)$ and $L^cMoO_2(OPh)$ complexes were prepared similarly from L^bMoO_2Cl (yield 71%) and L^cMoO_2Br (yield 97%; column loading solvent CH_2Cl_2; column eluant THF), but the reactions were carried out at room temperature in CH_2Cl_2 (2 days for the L^b complex and 16 h for the L^c complex). The complexes were recrystallized from CH_2Cl_2/pentane and CH_2Cl_2/hexane, respectively.

$L^cMoO_2(OPh)$: Anal. Calcd for $C_{18}H_{24}BN_9MoO_3$: C, 41.48; H, 4.64; N, 24.19. Found: C, 41.34; H, 4.59; N, 24.08.

$L^aMoO_2(SR)$ (R = Ph, CH_2Ph, Pr^i). $L^aMoO_2(SPh)$ was prepared as follows: L^aMoO_2Br (0.5 g, 1.0 mmol) was dissolved in dry, degassed CH_2Cl_2 (20 mL). A mixture of PhSH (0.22 mL, 2.0 mmol) and Et_3N (0.55 mL, 4.0 mmol) in toluene (2 mL) was added. The solution turned dark brown rapidly. After being stirred at room temperature for 2 h, the solution was evaporated to small volume and chromatographed on silica gel using CH_2Cl_2 as eluant. The first dark brown fraction was collected and the complex recrystallized from CH_2Cl_2/MeOH. Yield: 0.48 g (90%). Orange $L^aMoO_2(SCH_2Ph)$ was prepared similarly, in a yield of 74%. The method for the orange $L^aMoO_2(SPr^i)$ was similar, but the reaction mixture was heated at 50 °C for 24 h. The yield was 33%.

$L^bMoO_2(SPh)$. The procedure followed that for $L^aMoO_2(SPh)$. Yield: 82%. Anal. Calcd for $C_{24}H_{33}BN_6MoO_2S$: C, 50.01; H, 5.77; N, 14.58; S, 5.56. Found: C, 49.97; H, 5.72; N, 14.70; S, 5.71.

Table 3. Crystallographic Data for $L^aMoO_2(SPh)$, $L^bMoO_2(OMe)$, and $L^cMoO_2(SPh)$

	$L^aMoO_2(SPh)$	$L^bMoO_2(OMe)$	$L^cMoO_2(SPh)$
formula	$C_{21}H_{27}MoBN_6O_2S$	$C_{19}H_{31}MoBN_6O_3$	$C_{18}H_{24}MoBN_9O_2S$
color	burgundy red	colorless	dark red
fw	534.3	498.24	537.3
size, mm	0.20 × 0.45 × 0.50	0.50 × 0.33 × 0.24	0.33 × 0.22 × 0.04
a, Å	18.265(6)	30.365(4)	7.9302(13)
b, Å	8.110(3)	8.373(1)	16.627(2)
c, Å	18.299(3)	19.646(2)	17.543(2)
β, deg	117.06(2)	113.28(1)	
V, Å^3	2414(1)	4588(1)	2313.1(9)
Z	4	8	4
space group	$P2_1/c$	$C2/c$	$P2_12_12_1$
ρ, g cm^{-3}	1.47	1.41	1.543
μ, cm^{-1}	6.4	5.9	6.53
scan method	$\omega/2\theta$	$\omega/2\theta$	$\omega/2\theta$
data	4728	4420	6066
unique data	4241	4028	4068
$2\theta_{max}$, deg	50	50	50
weights (w)	$4F_o^2/\sigma^2(F_o^2)$	$4F_o^2/\sigma^2(F_o^2)$	$k[\sigma^2(F_o) + gF_o^2]^{-1}$
data refined	2964 ($F_o^2 \geq 3\sigma(F_o^2)$)	3721 ($F_o^2 \geq 3\sigma(F_o^2)$)	3681 ($F_o^2 \geq 2\sigma^2(F_o^2)$)
R	0.043	0.027	0.039
R_w	0.054	0.046	0.045
shift/esd	0.01	0.001	0.001
max diff peak, e Å^{-3}	1.22	0.45	1.30

$L^cMoO_2(SR)$ (R = Ph, CH_2Ph, Pr^i). The procedure was similar to that for $L^aMoO_2(SPh)$. The reactions were monitored by thin-layer chromatography (reactions complete after 2 h (R = Ph, CH_2Ph) and 15 h (R = Pr^i)). The solutions were loaded onto a silica gel column prepared using CH_2Cl_2. The products were eluted with THF as purple-brown (R = Ph) or orange (R = CH_2Ph, Pr^i) fractions and recrystallized from CH_2Cl_2/hexane. Respective yields were 88, 57, and 71%.

$L^cMoO_2(SPh)$: Anal. Calcd for $C_{18}H_{24}BN_9MoO_2S$: C, 40.24; H, 4.50; N, 23.46; S, 5.97. Found: C, 40.32; H, 4.54; N, 23.38; S, 6.05.

$(Bu^n_4N)_2[MoOS_3]$. To a mixture of $L^aMoO_2(SCH_2Ph)$ (0.20 g, 0.36 mmol) and Bu^n_4NSH (0.40 g, 1.5 mmol) was added THF (5 mL). The green solution was stirred at room temperature for 10 h and then stored at −15 °C. Yellow crystals of excess Bu^n_4NSH which precipitated overnight were filtered off. After the green filtrate was kept at −15 °C for 1 week, red-orange crystals formed and were characterized as the salt $(Bu^n_4N)_2[MoOS_3]$. Anal. Calcd for $C_{32}H_{72}N_2MoOS_3$: C, 55.46; H, 10.47; S, 13.88. Found: C, 55.30; H, 10.41; S, 13.75. IR (Nujol mull): ν(MoO) 862 s, ν(MoS) 469 s, br. ^{1}H NMR ($CDCl_3$): δ 0.96 (t, 3H, J = 7.2 Hz), 1.44 (m, 2H, J = 7.2 Hz), 1.58 (m, 2H), 3.33 (m, 2H).

Physical Techniques. Infrared spectra were recorded on a Bio-Rad Spec 3200 Fourier transform IR spectrophotometer using KBr disks. Proton NMR spectra were recorded on a Varian Unity-300 spectrometer using $CHCl_3$ as internal reference (δ = 7.24). EPR spectra were obtained on a Varian E-9 spectrometer using 1,1-diphenyl-2-picrylhydrazyl as reference.

The electrochemical experiments were performed at a glassy carbon disk (~0.07 cm^2) working electrode on a Cypress CS-1087 electrometer with a CYSY-1R potentiostat, using 0.2 M $Bu^n_4NBF_4$ as supporting electrolyte. The reference electrode used consisted of a $Ag/AgNO_3$ (0.01M in MeCN) electrode incorporated into a salt bridge containing supporting electrolyte to minimize Ag^+ contamination of the solution. The electrode was calibrated with the couple $[FeCp_2]^+/[FeCp_2]$.[31] $E_{1/2}$ for this couple is 0.100 V in MeCN. Potentials are quoted with respect to SCE by addition of 0.290 V in MeCN to the observed potentials since $E_{1/2}([FeCp_2]^+/[FeCp_2])$ is 0.39 V *vs* SCE in MeCN.[32] The auxiliary electrode was a platinum wire.

Before sample solutions were prepared, the electrolyte solution was examined by cyclic voltammetry to ensure no electrochemically active species were present within the potential window of the solvents. The sample solutions were purged of oxygen by purified dinitrogen prior to the measurements.

Generation of EPR Signals: EPR Measurements. By Electrochemical Reduction. The EPR electrolysis cell used was a semi-micro (*ca.* 0.2 mL) electrolysis cell compatible with an X-band EPR sample tube.[33] The cell featured platinum working and auxiliary electrodes and a silver/silver chloride reference electrode. The latter consisted of a quartz capillary containing a saturated solution of LiCl in CH_2Cl_2 to maintain a constant potential. Contact with the sample solution was made through an asbestos plug at the end of the capillary. The working and reference electrodes were orientated to provide the minimum possible separation to reduce the large ohmic drop and consequent loss of control of potential. The cell design enabled monitoring by cyclic voltammetry before electrolysis to ensure sample and cell viability.

Reduction of L^aMoO_2X (from 5 to 10 mM, depending on the solubility, 0.2 mL) was carried out in THF, with 0.2 M $Bu^n_4NBF_4$ as electrolyte, at *ca.* −42 °C using a BAS SP-2 potentiostat and a BAS CV-27 voltammograph. Reduction was performed at a potential 0.1 V more negative than the reduction peak and was continued until the spectra ceased growing (*ca.* 2 h). Frozen-solution spectra were obtained by lowering the temperature to *ca.* −135 °C after reduction at −42 °C.

By Bu^n_4NSH Reduction. The Bu^n_4NSH used was obtained from Fluka and was stored and dispensed in an inert-atmosphere drybox. An anaerobic solution of Bu^n_4NSH (0.07 M) in THF/MeCN (10/1) was added to solid $LMoO_2X$ to give a final concentration of 10 mM in molybdenum. The solution turned green immediately. The green solution was transferred into a Schlenk EPR tube under anaerobic conditions, frozen as quickly as possible (~3 min) for the measurement of the initial frozen-solution EPR spectrum, and then thawed for the corresponding solution spectrum. The subsequent reaction was followed by EPR. The reduction was complete within several minutes, and oxo−thio exchange, where it occurred, was complete essentially after *ca.* 10 h.

Crystal Structure Determinations. Single crystals of $L^aMoO_2(SPh)$ and $L^bMoO_2(OMe)$ suitable for X-ray structural analysis were grown by slow diffusion of methanol into solutions of the complexes in dichloromethane. For $L^cMoO_2(SPh)$, hexane was allowed to diffuse into a toluene solution of the complex.

Crystallographic data are given in Table 3 and positional parameters in Tables 4−6. Data were collected on Enraf-Nonius CAD4 diffractometers using Mo K$\bar{\alpha}$ radiation (graphite crystal monochromator), λ = 0.710 73 Å. The data were corrected for Lorentz and polarization effects, but not for extinction. The data for $L^aMoO_2(SPh)$ and $L^bMoO_2(OMe)$ were not corrected for absorption. Neutral-atom scattering

(31) Gagné, R. R.; Koval, C. A.; Lisensky, G. C. *Inorg. Chem.* **1980**, *19*, 2854.
(32) Bashkin, J. K.; Kinlen, P. J. *Inorg. Chem.* **1990**, *29*, 4507.
(33) Bagchi, R. N.; Bond, A. M.; Colton, R. *J. Electroanal. Chem. Interfacial Electrochem.* **1986**, *199*, 297.

Table 4. Positional Parameters for $L^aMoO_2(SPh)$

atom	*x/a*	*y/b*	*z/c*
Mo	0.23678(2)	0.06104(6)	0.30441(2)
O(1)	0.1834(2)	0.1758(5)	0.2189(2)
O(2)	0.2569(2)	−0.1145(5)	0.2659(2)
N(11)	0.1280(2)	−0.0409(5)	0.3067(2)
N(12)	0.1119(2)	−0.0365(5)	0.3730(2)
N(21)	0.2066(2)	0.2619(5)	0.3754(2)
N(22)	0.1830(2)	0.2267(5)	0.4355(2)
N(31)	0.2929(2)	−0.0562(6)	0.4330(2)
N(32)	0.2558(2)	−0.0438(5)	0.4835(2)
C(13)	0.0403(3)	−0.1140(7)	0.3537(3)
C(14)	0.0103(3)	−0.1696(7)	0.2740(3)
C(15)	0.0654(3)	−0.1220(7)	0.2464(3)
C(16)	0.0056(3)	−0.1336(9)	0.4122(3)
C(17)	0.0615(3)	−0.1505(8)	0.1638(3)
C(23)	0.1681(3)	0.3684(7)	0.4647(3)
C(24)	0.1806(3)	0.4954(7)	0.4230(3)
C(25)	0.2043(3)	0.4257(7)	0.3675(3)
C(26)	0.1421(3)	0.3734(9)	0.5306(3)
C(27)	0.2227(4)	0.5136(7)	0.3062(3)
C(33)	0.2979(3)	−0.1344(8)	0.5515(3)
C(34)	0.3623(4)	−0.2041(8)	0.5449(3)
C(35)	0.3585(3)	−0.1558(8)	0.4714(3)
C(36)	0.2732(4)	−0.145(1)	0.6188(3)
C(37)	0.4138(3)	−0.2024(9)	0.4363(4)
S	0.36783(8)	0.1965(2)	0.35597(8)
C(1)	0.3854(3)	0.2307(8)	0.2691(3)
C(2)	0.3550(3)	0.1356(8)	0.2004(3)
C(3)	0.3741(3)	0.170(1)	0.1376(4)
C(4)	0.4219(4)	0.300(1)	0.1408(4)
C(5)	0.4532(4)	0.395(1)	0.2094(4)
C(6)	0.4346(3)	0.3675(9)	0.2739(4)
B	0.1736(3)	0.0475(8)	0.4535(3)

Table 5. Positional Parameters for $L^bMoO_2(OMe)$

atom	*x/a*	*y/b*	*z/c*
Mo	0	0.18091(2)	0.11311(1)
O(1)	−0.11010(5)	0.3237(2)	0.10108(8)
O(2)	−0.17410(5)	0.2763(2)	0.16147(7)
O(3)	−0.19547(5)	0.1679(1)	0.01890(7)
N(11)	−0.08783(5)	0.1009(2)	0.21641(7)
N(12)	−0.07257(5)	−0.0537(2)	0.22816(7)
N(21)	−0.10803(5)	−0.0042(2)	0.06531(7)
N(22)	−0.09094(5)	−0.1454(2)	0.09918(8)
N(31)	−0.17651(5)	−0.0607(2)	0.13635(8)
N(32)	−0.14900(6)	−0.1950(2)	0.15780(9)
C(1)	−0.22154(7)	0.0524(3)	−0.0331(1)
C(13)	−0.03552(6)	−0.0631(2)	0.29342(9)
C(14)	−0.02637(7)	0.0851(3)	0.3249(1)
C(15)	−0.05969(7)	0.1863(2)	0.2758(1)
C(16)	−0.06739(8)	0.3607(3)	0.2840(1)
C(17)	−0.10398(9)	0.3876(3)	0.3181(1)
C(18)	−0.0212(1)	0.4444(3)	0.3317(2)
C(23)	−0.07066(8)	−0.2268(3)	0.0608(1)
C(24)	−0.07363(8)	−0.1372(3)	0.0005(1)
C(25)	−0.09798(7)	0.0017(3)	0.0044(1)
C(26)	−0.11083(8)	0.1400(4)	−0.0482(1)
C(27)	−0.0667(1)	0.2449(5)	−0.0332(2)
C(28)	−0.13188(9)	0.0820(5)	−0.1285(1)
C(33)	−0.17484(8)	−0.3151(2)	0.1666(1)
C(24)	−0.21982(7)	−0.2614(3)	0.1519(1)
C(25)	−0.22029(6)	−0.1004(2)	0.13267(9)
C(36)	−0.26082(6)	0.0170(3)	0.1135(1)
C(37)	−0.30804(8)	−0.0595(4)	0.0630(2)
C(38)	−0.26404(9)	0.0774(4)	0.1844(1)
B	−0.09609(8)	−0.1875(2)	0.1716(1)

factors for $L^aMoO_2(SPh)$ and $L^bMoO_2(OMe)$ were taken from the literature,[34a] the values being corrected for anomalous dispersion.[34b] For $L^cMoO_2(SPh)$ the atomic scattering factors of C, H, B, N, O, and S were those incorporated in the SHELX-76 program system.[35] Coefficients for the scattering curves for atomic Mo were obtained from

(34) *International Tables for X-Ray Crystallography*; Kynoch: Birmingham, U.K., 1974: (a) Vol. IV, p 99; (b) Vol. IV, p 149.

Table 6. Positional Parameters for $L^cMoO_2(SPh)$

atom	*x/a*	*y/b*	*z/c*
Mo	−0.17504(5)	0.00797(2)	−0.13254(2)
O(1)	−0.3018(5)	0.0611(2)	−0.1925(2)
O(2)	−0.0121(4)	0.0715(2)	−0.1146(2)
N(11)	−0.0567(5)	−0.0582(2)	−0.2254(2)
N(12)	−0.0303(5)	−0.1403(2)	−0.2273(2)
C(13)	0.0638(6)	−0.1548(3)	−0.2878(3)
N(14)	0.0990(6)	−0.0883(3)	−0.3273(2)
C(15)	0.0197(7)	−0.0300(3)	−0.2873(3)
C(16)	0.1266(8)	−0.2359(3)	−0.3100(3)
C(17)	0.0193(9)	0.0555(3)	−0.3091(4)
N(21)	−0.3483(4)	−0.1013(2)	−0.1472(2)
N(22)	−0.2924(5)	−0.1786(2)	−0.1587(2)
C(23)	−0.4266(6)	−0.2239(3)	−0.1749(3)
N(24)	−0.5667(5)	−0.1815(3)	−0.1726(3)
C(25)	−0.5157(6)	−0.1057(3)	−0.1576(3)
C(26)	−0.4205(7)	−0.3117(3)	−0.1920(3)
C(27)	−0.6292(6)	−0.0360(4)	−0.1550(4)
N(31)	−0.0184(5)	−0.0901(2)	−0.0681(2)
N(32)	−0.0143(5)	−0.1695(2)	−0.0899(2)
C(33)	0.0914(6)	−0.2082(3)	−0.0420(3)
N(34)	0.1555(6)	−0.1583(2)	0.0080(2)
C(35)	0.0886(7)	−0.0866(3)	−0.0097(3)
C(36)	0.1270(8)	−0.2956(3)	−0.0471(3)
C(37)	0.1307(8)	−0.0115(4)	0.0325(4)
S	−0.3231(2)	0.01565(8)	−0.01357(8)
C(1)	−0.2799(7)	0.1133(4)	0.0232(3)
C(2)	−0.3316(10)	0.1810(3)	−0.0141(4)
C(3)	−0.3089(13)	0.2559(5)	0.0177(5)
C(4)	−0.2287(12)	0.2646(6)	0.0861(6)
C(5)	−0.1721(11)	0.1975(6)	0.1240(4)
C(6)	−0.2018(10)	0.1204(5)	0.0941(4)
B	−0.0987(7)	−0.1948(3)	−0.1638(3)

ref 36a; corrections were made for anomalous dispersion.[36b] Analyses of variance after final refinements showed no unusual features.

$L^aMoO_2(SPh)$. Accurate cell parameters were obtained from least-squares refinement of the setting angles of 23 reflections in the range $20 < 2\theta < 30°$. Two reflections monitored after every 3600 s of X-ray exposure time showed no intensity variation. The structure was solved by using a combination of Patterson and difference electron density syntheses. The full-matrix least-squares refinement allowed anisotropic temperature factors for each of the non-hydrogen atoms; all hydrogen atoms were included with fixed isotropic temperature factors and constrained to geometrical estimates using the riding model. The largest peak in the final difference map was close to the Mo atom. Calculations were performed using MolEN software.[37]

$L^bMoO_2(OMe)$. Accurate cell parameters were obtained from least-squares refinement of the setting angles of 25 reflections in the range $17 < 2\theta < 22°$. The crystal showed systematic absences consistent with the space groups *Cc* and *C2/c*, and a satisfactory solution was obtained in the latter. Three reflections monitored every 3600 s during X-ray exposure time showed no intensity variation. The structure was solved by using a combination of Patterson map and difference synthesis. The full-matrix least-squares refinement allowed anisotropic temperature factors for each of the non-hydrogen atoms; hydrogen atoms were included with fixed isotropic temperature factors and coordinates constrained by the riding model. Calculations were performed using SDP/VAX software.[38]

$L^cMoO_2(SPh)$. Accurate values of the unit cell parameters and crystal orientation were obtained by a least-squares refinement of the angular settings of 25 carefully centered reflections. Three reflections, monitored every 9600 s X-ray exposure time, showed a 5% decrease;

(35) Sheldrick, G. M. *SHELX-76: Program for Crystal Structure Determination*; University of Cambridge: Cambridge, U.K., 1976.

(36) *International Tables for X-ray Crystallography*; Kluwer Academic Publishers: Dordrecht, The Netherlands, 1993: (a) Vol. C, p 500; (b) Vol. C, p 219.

(37) *MolEN: An Interactive Structure Solution Procedure*; Enraf-Nonius: Delft, The Netherlands, 1990.

(38) Frenz, B. A. In *Computing in Crystallography*; Schenk, H., Olthof-Hazelkamp, R., vanKonigsveld, H., Bassi, G. C., Eds.; Delft University Press: Delft, The Netherlands, 1978; pp 64−71.

Table 7. Selected Bond Distances (Å) and Angles (deg)

	$L^aMoO_2(SPh)$	$L^bMoO_2(OMe)$	$L^cMoO_2(SPh)$
Mo−O(1)	1.696(4)	1.705(2)	1.702(4)
Mo−O(2)	1.702(4)	1.697(2)	1.698(3)
Mo−S/O(3)	2.402(2)	1.865(2)	2.398(2)
Mo−N(11)	2.169(4)	2.209(2)	2.178(4)
Mo−N(21)	2.302(4)	2.346(2)	2.292(3)
Mo−N(31)	2.301(4)	2.338(2)	2.341(4)
S/O(3)−C(1)	1.781(6)	1.402(3)	1.780(7)
O(1)−Mo−O(2)	102.6(2)	103.78(8)	103.9(2)
Mo−S/O(3)−C(1)	105.8(2)	139.7(1)	105.6(2)

the data were corrected in accordance with this variation. Absorption corrections were evaluated by Gaussian integration. The structure was solved using a combination of Patterson map, direct methods, and difference electron density syntheses. All of the hydrogen atoms were included in the refinement, constrained at geometrical estimates, apart from the boron hydrogen, which was refined. Full-matrix least-squares refinement, with anisotropic temperature factors applied to each of the non-hydrogen atoms and a common isotropic temperature factor being assigned to the hydrogens on each carbon, was carried out with a weighting scheme of the type $k[\sigma^2(F) + gF^2]^{-1}$ until the shift/esd of any parameter was less than 0.001. At convergence, R = 0.041, R_w = 0.049, k = 1.279, and g = 0.000 57 for one enantiomorph and R = 0.039, R_w = 0.045, k = 1.224, and g = 0.000 52 for the other, indicating that the latter was probably the preferred configuration. The maximum peak height in the final difference map was 1.30 e Å^{-3}, close to the Mo atom. Calculations were performed using SHELX-76[35] and SHELXS-86[39] software.

Results

Syntheses and Spectroscopic Data. A range of dioxo−Mo(VI) complexes of the type $LMoO_2X$ were prepared. Improved syntheses for several known L^aMoO_2X complexes were developed and then adapted to the synthesis of related L^b and L^c species. The crystalline, air-stable complexes were generally white or pale yellow, the orange or dark brown thiolate complexes being exceptions to the rule. The L^a and L^b complexes exhibited good solubility in chlorinated solvents, acetonitrile, and THF but were insoluble in alcohols, diethyl ether, and hydrocarbons. The L^c complexes were highly soluble in alcohols, chlorinated solvents, aromatic hydrocarbons, acetone, THF, and acetonitrile but were insoluble in alkanes.

The infrared spectra of the complexes (Table 1) exhibited two strong bands in the ranges 940−920 and 910−890 cm^{-1}; these were assigned to the symmetric and asymmetric vibrational modes, respectively, of the *cis*-$[MoO_2]^{2+}$ fragment. The frequencies of these bands were observed to vary according to L, with $\nu(L^cMoO_2X) > \nu(L^bMoO_2X) > \nu(L^aMoO_2X)$. Bands characteristic of the other ligands dominated other regions of the infrared spectra; for complexes of L^b, a broad, single ν(CN) band at 1506 cm^{-1} was observed in all cases.[40] All complexes exhibited ^{1}H NMR spectra (Table 2) consistent with molecular C_s symmetry in solution. In their complexes, the tripodal N-donor ligands exhibited resonance patterns as follows: four singlet methyl resonances (6:6:3:3 integration) and two methine resonances (2:1 integration) for L^aMoO_2X complexes; three doublet methyl resonances (6:6:6 integration), two septet isopropyl methine resonances (2:1 integration), and four doublet ring methine resonances (2:2:1:1 integration) for L^bMoO_2X complexes; four singlet methyl resonances (6:6:3:3 integration) for L^cMoO_2X complexes. The methyl resonances of particular L^c complexes were deshielded relative to the resonances of their L^a analogues.

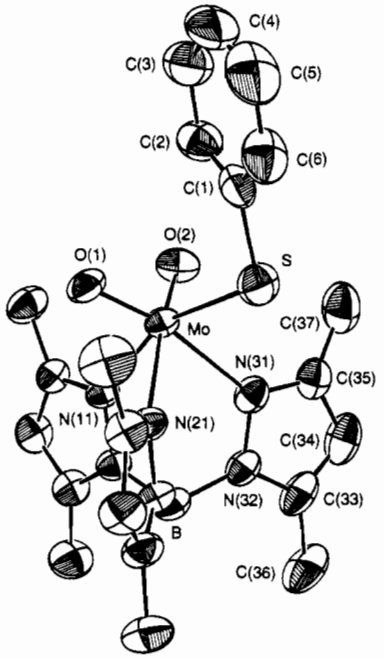

Figure 1. Molecular structure and crystallographic numbering scheme for $L^aMoO_2(SPh)$. The numbering of atoms in the residues containing N(11) and N(21) parallels that shown for the residue containing N(31).

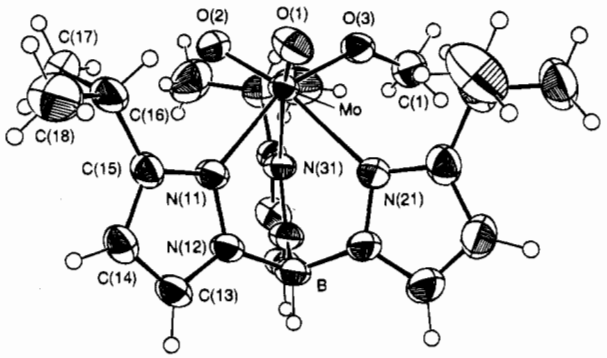

Figure 2. Molecular structure and crystallographic numbering scheme for $L^bMoO_2(OMe)$. The numbering of atoms in the residues containing N(21) and N(31) parallels that shown for the residue containing N(11).

Crystal Structures. Selected bond distances and angles for $L^aMoO_2(SPh)$, $L^bMoO_2(OMe)$, and $L^cMoO_2(SPh)$ are given in Table 7. Figures 1−3 provide views of the molecules and atom labeling schemes. All three molecules are six-coordinate monomers with distorted octahedral geometries and local C_s symmetry; the coordination spheres are composed of the facially tridentate L ligands, a pair of terminal oxo ligands, and an SPh^- or OMe^- ligand. The monodentate ligands are mutually *cis* as dictated by the facial coordination of L. The presence of the hydrotris(3-isopropylpyrazolyl)borate ligand in $L^bMoO_2(OMe)$ was confirmed by crystallography. The Mo atoms are displaced from the midpoint of the equatorial planes defined by O(1), O(2), N(21), and N(31) toward the oxo ligands. The Mo=O

(39) Sheldrick, G. M. *Acta Crystallogr., Sect. A* **1990**, *46*, 467.

(40) Crystallographic characterization of $L'MoO(S_2PPr^i_2)$ and $L'MoS(S_2PPh_2)$ [L′ = hydrobis(3-isopropylpyrazolyl)(5-isopropylpyrazolyl)borate] revealed that L^b had undergone a borotropic shift during the synthesis of the former from $MoO(S_2PPr^i_2)_2$ and KL^b in refluxing toluene. Complexes of L′ may be distinguished from those of L^b by the following diagnostic features: IR, two bands in the ν(CN) region (one for L^b complexes); ^{1}H NMR, the methine protons of the 5-isopropylpyrazole group are uniquely shielded. For related $L'MoO(S_2PR_2)$ complexes, the 5-isopropyl methine (δ ca. 3.1) and 4-methine (δ 5.6) resonances are considerably shielded relative to those of the complexes reported herein (δ > 3.45 and δ > 6.06, respectively): Laughlin, L. J.; Colmanet, S.; Young, C. G. Unpublished results. Other examples of borotropic shifts involving L^b may be found in ref 26 and in: Cano, M.; Heras, J. V.; Jones, C. J.; McCleverty, J. A.; Trofimenko, S. *Polyhedron* **1990**, *9*, 619.

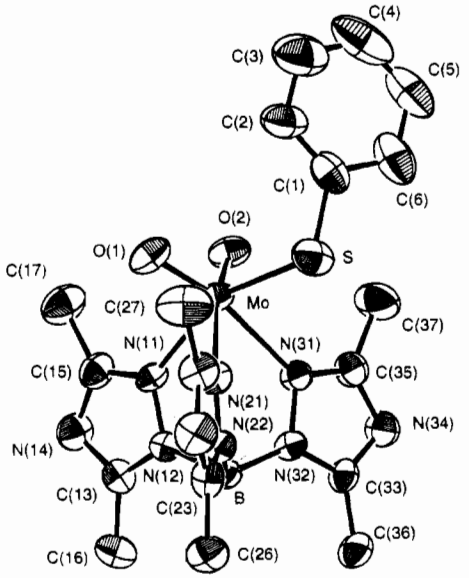

Figure 3. Molecular structure and crystallographic numbering scheme for $L^cMoO_2(SPh)$.

Table 8. Electrochemical Data in MeCN at 22 °C[a]

	$E_{1/2}$, V			ΔE_{pp}, mV			I_{pa}/I_{pc}		
X	L^a	L^b	L^c	L^a	L^b	L^c	L^a	L^b	L^c
Cl	−0.62[b]	−0.50	−0.39	230[b]	82	70	0.50[b]	0.77	0.99
Br	−0.48	−0.45	−0.38	*c*	*c*	*c*	*c*	*c*	*c*
SCN	−0.42			75			0.87		
OMe	−1.13	−1.03	−0.89	76	73	75	0.94	1.00	0.98
OEt	−1.14	−1.05		76	76		0.96	1.00	
OPr^n	−1.15			80			0.96		
OPh	−0.88	−0.78	−0.66	73	72	72	0.99	1.02	0.97
SPh	−0.76	−0.66	−0.52	66	71	73	1.02	1.00	0.98
SPr^i	−0.91		−0.67	68		69	1.02		0.98
SCH_2Ph	−0.84		−0.60	66		60	1.02		0.97

[a] Conditions: glassy-carbon; scan rate = 100 mV/s; 0.2 M Bu_4NBF_4; vs SCE. $E_{1/2}$(ferrocene): +0.39 V in MeCN; [complex] = 0.5 mM. [b] In CH_2Cl_2. [c] The observed wave is completely irreversible.

Table 9. Cyclic Voltammetric Data for L^aMoO_2X in MeCN

complex	v, mV s^{-1}	E_{pa} (V)	E_{pc} (V)	ΔE_{pp} (mV)	I_{pc} (μA)	I_{pa}/I_{pc}
$FeCp_2$	20	+0.423	+0.355	68	15.0	0.97
(1.0 mM)	50	+0.425	+0.354	71	22.9	0.97
	80	+0.424	+0.357	67	28.8	0.98
	100	+0.423	+0.356	67	31.6	0.98
	200	+0.423	+0.354	69	44.0	0.99
	350	+0.424	+0.352	73	57.6	0.99
	500	+0.429	+0.350	79	68.2	0.99
X = SPh	20	−0.725	−0.794	69	5.60	1.00
(0.5 mM)	50	−0.722	−0.795	73	8.50	1.04
	80	−0.725	−0.792	67	10.5	1.02
	100	−0.726	−0.792	66	11.8	1.04
	200	−0.725	−0.793	68	16.1	1.05
	350	−0.722	−0.794	72	21.2	1.07
	500	−0.719	−0.795	76	25.3	1.09
X = SPr^i	50	−0.879	−0.953	74	14.3	1.04
(1.0 mM)	80	−0.882	−0.950	68	17.9	1.01
	100	−0.884	−0.952	68	19.8	1.02
	200	−0.880	−0.953	73	27.7	1.00
	350	−0.881	−0.957	76	36.1	1.01
	500	−0.877	−0.958	81	42.7	1.01

bond distances and O=Mo=O angles were in the ranges 1.696(4)−1.705(2) Å (average 1.700 Å) and 102.6(2)−103.9(2)° (average 103.4°), respectively. The Mo−N(11) bond, which is *trans* to the X ligand, is the shortest of the Mo−N bonds in each case. The Mo−N(21) and Mo−N(31) bonds, which are *trans* to the oxo ligands, are up to 0.16 Å longer than the Mo−N(11) bonds. The Mo−S−C(1) angles of $LMoO_2(SPh)$, *ca.* 105.7° in both cases, are considerably smaller than the Mo−O-C(1) angle of 139.7(1)° for $L^bMoO_2(OMe)$. The SPh^- ligands are oriented so that the phenyl ring projects into the pocket formed by the methyl groups of L^a and L^c and overlies the two Mo=O bonds. The OMe^- ligand lies between a pair of ligand isopropyl groups with the methyl group directed away from the oxo ligands.

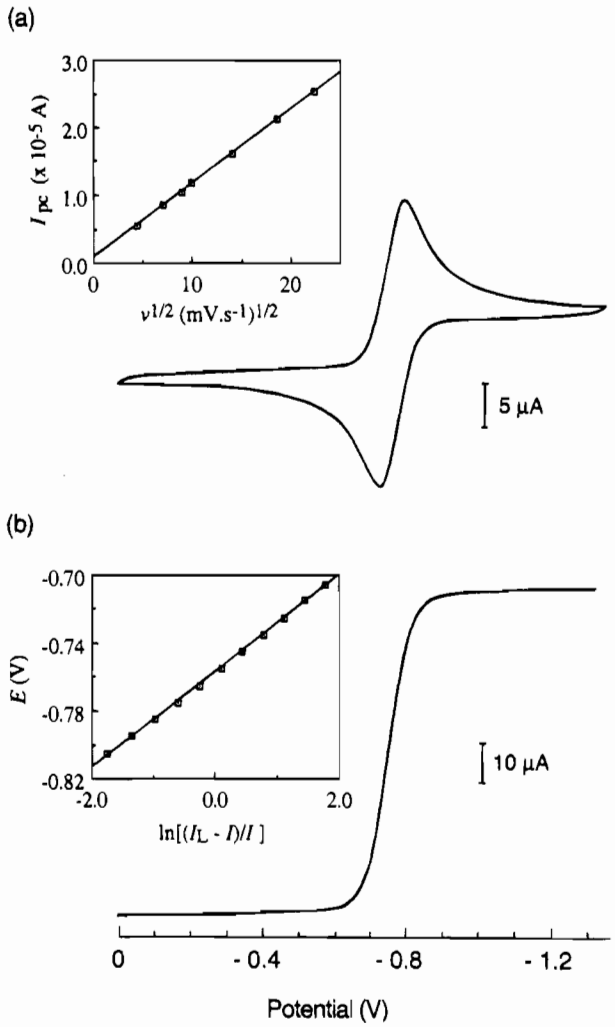

Figure 4. (a) Cyclic voltammogram of $L^aMoO_2(SPh)$ (0.5 mM) in MeCN (v = 100 mV s^{-1}; 0.2 M $Bu^n_4NBF_4$). Inset: plot of I_{pc} versus $v^{1/2}$. (b) Rotating disk voltammogram of the same solution (v = 50 mV s^{-1}; ω = 262 s^{-1}). Inset: plot of E versus $\ln[(I_L - I)/I]$.

Electrochemistry. Electrochemical data are summarized in Tables 8 and 9, and results pertaining to $L^aMoO_2(SPh)$ are shown in Figure 4. With the exception of L^cMoO_2Cl, the $LMoO_2X$ (X = Cl, Br, SCN) complexes exhibited an irreversible reduction process at normal scan rates (20−500 mV s^{-1}). All other complexes exhibited chemically reversible behavior ($I_{pa}/I_{pc} > 0.9$) for the only reduction process observed in acetonitrile in the range +1.0 to −2.0 V (*vs* SCE). In many cases, the behavior is electrochemically reversible:[41] both E_p and ΔE_p were independent of scan rate v; ΔE_p values were close to that observed for the standard couple $[FeCp_2]^+/[FeCp_2]$ under the same conditions and close to 59 mV, the theoretical value; plots of I_{pc} vs $v^{1/2}$ were linear passing through the origin (see Figure 4a). Rotating disk voltammetry showed the limiting current I_L to be proportional to $\omega^{1/2}$ (ω, rotation rate) while a plot of E vs $\ln[(I_L - I)/I]$ was linear, with intercept $E_{1/2}$ identical to the values

(41) Brown, E. R.; Large, R. F. In *Techniques of Chemistry*; Weissberger, Rossiter, Eds.; Wiley: New York, 1971; Vol. 1, Chapter 6.

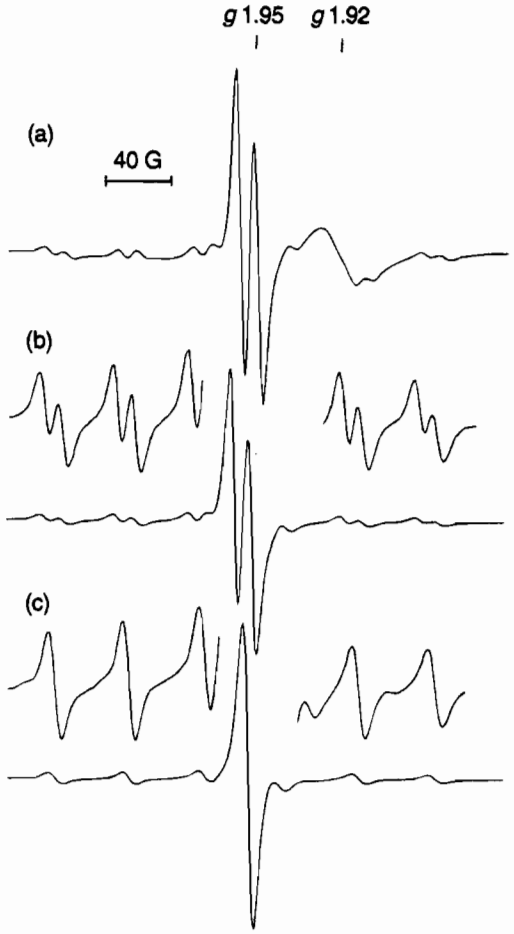

Figure 5. EPR spectra generated by electrochemical reduction of $L^aMoO_2(SPh)$ at 293 K: (a) 0.2 M $Bu^n_4NBF_4$ in THF dried over activated alumina (the broad feature is due to $[L^aMoO_2(SPh)]^-$); (b) 1 M ^1H_2O and 0.2 M $Bu^n_4NBF_4$ in THF; (c) 1 M ^2H_2O and 0.2 M $Bu^n_4NBF_4$ in THF.

given in Table 8 and a slope similar to that for the known one-electron couple $[FeCp_2]^+/[FeCp_2]$ (see, for example, Figure 4b).

Generation of Molybdenum(V) Species. Reduction at potentials guided by the data in Table 8 was carried out in an electrochemical cell compatible with the normal cylindrical sample cells housed in the cavity of an EPR spectrometer.[22] When dissolved in electrolyte (0.2 M $Bu^n_4NBF_4$ in THF) carefully dried with activated alumina at room temperature, the complexes $L^aMo^{VI}O_2X$ (X = SPh, SCH_2Ph) produced initially a very broad (>2 G) signal at $g \approx 1.92$; these signals are ascribed to $[L^aMo^VO_2X]^-$ species on the basis of spectral comparisons.[22-24] Upon more extended electrolysis, the broad signal was replaced by a doublet ($g = 1.95$) featuring coupling to $^{95,97}Mo$ ($I = 5/2$, 25.2 atom %) and ^1H ($I = 1/2$) (Figure 5a). In wet solvents, closely related doublet signals were cleanly generated upon reduction of all $LMo^{VI}O_2X$ complexes (e.g., Figure 5b,c); on the basis of spectral comparisons, these signals are ascribed to $L^aMo^VO(OH)X$ species.[22-24] For X = Br, additional coupling to $^{79,81}Br$ ($I = 3/2$) was detected in $L^aMo^VO(OH)Br$. Better spectral resolution was obtained using PPh_3 as reductant in wet THF (Figure 6).[42] Freezing of the solutions usually provided well-resolved anisotropic spectra. EPR parameters are summarized in Tables 10 and 11.

The broad signals of the $[LMo^VO_2X]^-$ species could be generated cleanly in THF/MeCN (9/1) solution by a 7 molar excess of Bu^n_4NSH, which provides reducing equivalents in a strongly basic solution (Figure 7; Table 12). Provided that the green solutions were frozen quickly after generation under anaerobic conditions, clean anisotropic spectra could be obtained (e.g., Figure 7b), but the detailed behavior depended upon ligand X. For X = OPh, SPh, and SPr^i, the signal was stable at room temperature for several days. For X = Cl, Br, NCS, and SCH_2-

(42) (a) Xiao, Z. Ph.D. Dissertation, La Trobe University, Bundoora, Australia, 1992. (b) Xiao, Z.; Enemark, J. H.; Young, C. G.; Wedd, A. G. Manuscript in preparation.

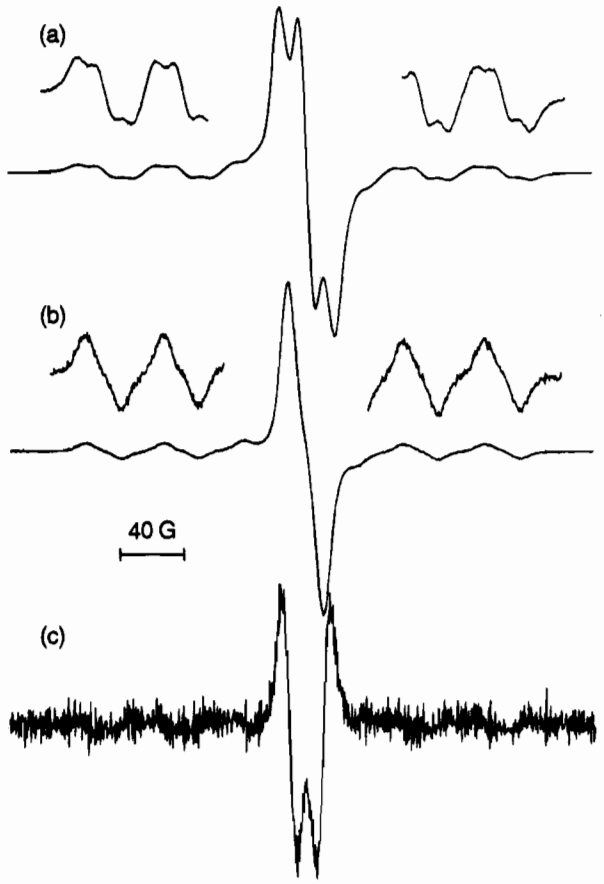

Figure 6. EPR spectra generated by the reaction of L^aMoO_2Br and PPh_3 at 293 K: (a) 1 M H_2O in THF; (b) 1 M ^2H_2O in THF. Spectrum c is a second-derivative representation of (b) showing $^{79,81}Br$ ($I = 3/2$) coupling.

Table 10. EPR Parameters for $L^aMoO(OH)X$ Generated in Water (1 M)/THF[a]

X	g_1[b]	g_2[b]	g_3[b]	g	$A(^{95,97}Mo)$[c]	$A(^1H)$[c]
Cl				1.942	46.8	13.0
	1.966[d]	1.946[d]	1.914[d]	1.942	46.8	
Br				1.949	47.2	11.7[e]
				1.949	47.0	
NCS				1.940	46.3	11.5
	1.966[d]	1.944[d]	1.922[d]	1.940	46.2	
OMe				1.939	47.2	10.1
	1.970	1.945	1.904	1.939	47.1	
OEt				1.938	47.1	10.1
	1.969	1.945	1.903	1.938	47.0	
OPr^n				1.938	47.1	9.6
	1.970	1.947	1.907	1.938	47.1	
OPh				1.938	47.4	11.2
	1.970	1.943	1.903	1.938	47.4	
SPh				1.950	42.8	12.5
	1.979	1.949	1.921	1.950	42.7	
SCH_2Ph				1.952	42.3	10.2
	1.982	1.950	1.927	1.952	42.3	

[a] Generated by electrochemical reduction of L^aMoO_2X complexes in THF/0.2 M Bu_4NBF_4/1.0 M water. Estimated errors in g values are ± 0.001 and in A are $\pm 0.3 \times 10^{-4}$ cm^{-1}. [b] Measured at 138 K. [c] Units: 10^{-4} cm^{-1}. [d] Generated by reactions of L^aMoO_2X with PPh_3 in toluene/D_2O, 77 K. [e] Coupling of $^{79,81}Br$ is observed.

Table 11. Comparison of EPR Data for LMoO(OH)X[a]

X	L^a			L^b			L^c		
	g	$A(^{95,97}Mo)$	$A(^1H)$	g	$A(^{95,97}Mo)$	$A(^1H)$	g	$A(^{95,97}Mo)$	$A(^1H)$
Cl	1.942	47.1	13.4	1.944	47.5	13.8	1.943	47.7	14.0
	1.944	47.2		1.944	47.6		1.944	47.9	
Br[b]	1.951	46.3	11.0	1.951	46.9	11.9	1.951	46.6	12.5
	1.951	46.5		1.951	46.9		1.952	46.8	
NCS	1.941	46.2	11.4						
	1.943	46.3							
OMe	1.938	47.5	10.6	1.939	47.7	10.2	1.939	47.7	10.7
	1.939	47.6		1.939	47.6		1.939	47.8	
OPh	1.938	47.7	11.1	1.938	48.2	11.6	1.939	48.3	11.7
	1.939	47.7		1.938	47.9		1.939	48.2	
SPh	1.951	42.9	11.5	1.952	43.3	12.4	1.951	42.4	11.4
	1.952	42.9		1.952	43.2		1.952	42.7	
SCH_2Ph	1.952	42.4	10.3				1.953	42.1	10.3
	1.952	42.4					1.953	42.1	
SPr^i	1.953	42.1	10.1				1.953	41.8	10.2
	1.953	42.3					1.953	41.7	

[a] Generated by reactions of $LMoO_2X$ in toluene/H_2O with PPh_3 at 295 K. Estimated errors in g values are ±0.001 and in A are ±0.3 × 10^{-4} cm^{-1}. Units for A: 10^{-4} cm^{-1}. [b] $^{79,81}Br$ coupling observed.

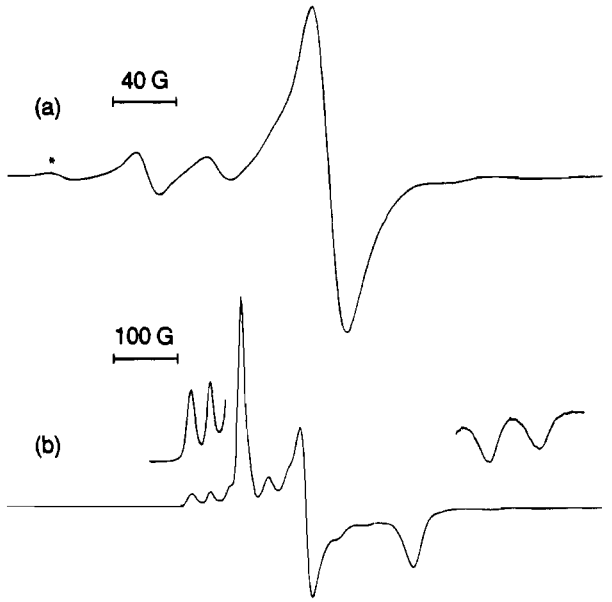

Figure 7. EPR spectra generated by the reaction of $L^aMoO_2(SPh)$ and a 7-fold excess of Bu^n_4NSH in THF/MeCN (10/1), recorded after 5 h: (a) 293 K; (b) 77 K. Asterisk: signal from Bu^n_4NSH solution.

Ph, the initial signal was replaced by another one of higher g and lower A values after 10 h (Figure 8). The new signals were characteristic of $[LMo^VOSX]^-$ complexes.[22-24] For X = OPh, SPh, and SPr^i, however, the strong EPR signal characteristic of $[LMoO_2X]^-$ remains the only EPR signal even after incubation at room temperature for 2 days. For $[L^bMoO_2Cl]^-$ and $[L^cMoO_2Cl]^-$, additional coupling to $^{35,37}Cl$ (I = $^3/_2$) was observed in one direction, but the expected hyperfine quartet was not fully resolved (Figure 9).

As a consequence of their lower $E_{1/2}$ values (Table 8), the alkoxide complexes did not react completely with Bu^n_4NSH. Reactions of L^aMoO_2X (X = Cl, SCH_2Ph) with Bu^n_4NSH (Mo:SH = 1:4) in THF on a preparative scale led to the slow formation of red-orange crystals of $(Bu^n_4N)_2[MoOS_3]$ upon standing of the green solution at −15 °C. Exposure of the green solution to air allowed isolation of a purple-brown complex $[L^aMo^VO]_2(\mu\text{-}O)(\mu\text{-}S_2)$.[30] The formation of this complex depended upon the reaction medium. Thus, reaction of L^aMoO_2Br with a limiting excess of Bu^n_4NSH in dichloromethane led to a rapid color change from yellow to purple-brown instead of green, indicating formation of $[L^aMo^VO]_2(\mu\text{-}O)(\mu\text{-}S_2)$.

Table 12. EPR Parameters for Anionic Species[a]

species	g_1[b]	g_2[b]	g_3[b]	g	A[c]	$W_{1/2}$, G
$[L^aMoO_2Cl]^-$	1.9936	1.9288	1.8343	1.917	44.9	26.0
$[L^bMoO_2Cl]^-$	1.9904	1.9268	1.8159			
$[L^cMoO_2Cl]^-$	1.9889	1.9260	1.8135			
$[L^aMoO_2Br]^-$	1.9935	1.9280	1.8341	1.917	44.5	25.8
$[L^bMoO_2Br]^-$	1.9939	1.9307	1.8283			
$[L^aMoO_2(NCS)]^-$	1.9939	1.9277	1.8350	1.917	44.6	25.4
$[L^aMoO_2(OMe)]^-$[d]	1.9889	1.9241	1.8311	1.911	44.4	25.0
$[L^aMoO_2(OPh)]^-$	1.9904	1.9243	1.8206	1.910	46.9	25.6
$[L^bMoO_2(OPh)]^-$	1.9902	1.9249	1.8129			
$[L^aMoO_2(SPh)]^-$	1.9915	1.9307	1.8388	1.920	41.2	22.0
$[L^bMoO_2(SPh)]^-$	1.9921	1.9349	1.8390			
$[L^aMoO_2(SPr^i)]^-$	1.9904	1.9320	1.8497	1.920	39.1	18.6
$[L^aMoO_2(SCH_2Ph)]^-$	1.9906	1.9313	1.8519	1.921	39.8	23.3
$[(L\text{-}N_2S_2)MoO_2]^-$[e]	1.9868	1.9158	1.8106			
$[L^aMoOSCl]^-$	2.0100	1.9304	1.8743	1.937	37.4	18.6
$[L^bMoOSCl]^-$	2.0112	1.9320	1.8680			
$[L^aMoOSBr]^-$	2.0106	1.9309	1.8750	1.938	37.1	18.3
$[L^bMoOSBr]^-$	2.0119	1.9331	1.8683			
$[L^aMoOS(NCS)]^-$	2.0104	1.9303	1.8743	1.937	36.6	17.8
$[L^aMoOS(SCH_2Ph)]^-$	2.0219	1.9478	1.8984	1.954	34.1	18.4
$[(L\text{-}N_2S_2)MoOS]^-$[e]	2.0165	1.9336	1.8885			

[a] Generated by reaction of $LMoO_2X$ species with 7-fold Bu^n_4NSH in THF/MeCN (9/1). Estimated errors in g values are ±0.0005 and in A are ±0.3 × 10^{-4} cm^{-1}. [b] Measured at 77 K. [c] Units: 10^{-4} cm^{-1}. [d] Weak intensity. [e] Adapted from ref 23: $(g_1, g_2, g_3) = (g_x, g_y, g_z)$.

Discussion

The salts KL^a and KL^b were prepared by methods described by Trofimenko *et al.*,[25,26] but the preparation of KL^c has not been described previously; it follows straightforwardly the synthesis of potassium hydrotris(1,2,4-triazol-1-yl)borate described by Trofimenko and others[43] (eq 1). The L^c ligand is

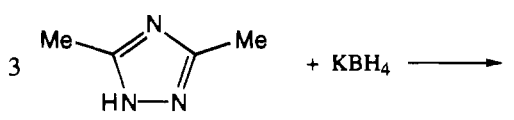

(1)

more electron withdrawing than the L^a and L^b ligands, as

(43) (a) Trofimenko, S. *J. Am. Chem. Soc.* **1967**, *89*, 3170. (b) Trofimenko, S. *Inorg. Synth.* **1970**, *12*, 99. (c) Lobbia, G. G.; Bonati, F.; Cecchi, P. *Synth. React. Inorg. Met.-Org. Chem.* **1991**, *21*, 1141. (d) Shiu, K.-B.; Lee, J. Y.; Wang, Y.; Cheng, M.-C.; Wang, S.-L.; Liao, F.-L. *J. Organomet. Chem.* **1993**, *453*, 211.

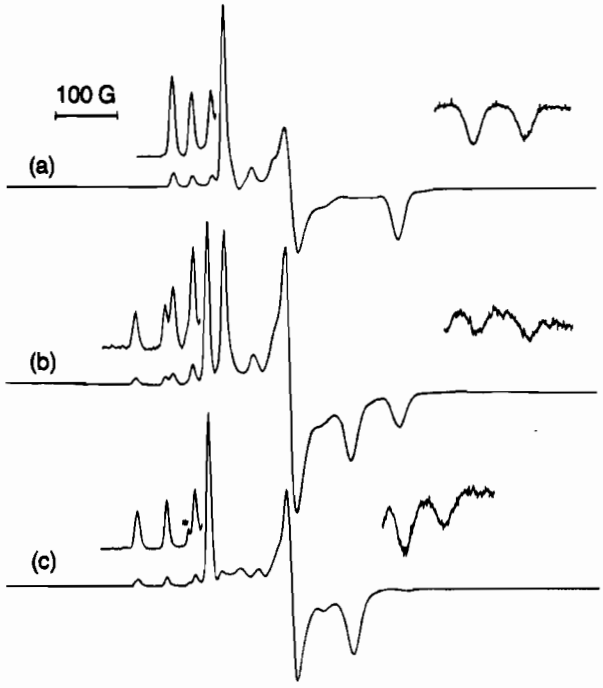

Figure 8. EPR spectra at 77 K generated by the reaction of L^aMoO_2Cl and a 7-fold excess of Bu^n_4NSH in THF/MeCN (10/1): (a) frozen within 4 min and recorded; (b) frozen after 2.5 h and recorded; (c) frozen after 10 h and recorded. Asterisk: signal from Bu^n_4NSH solution.

reflected in electrochemical results described herein and comparative studies of carbonyl–Mo complexes.[44]

Improved synthetic procedures for the isolation of the complexes L^aMoO_2X have been developed and extended to encompass a wider range of X ligands and complexes of L^b and L^c. The bromo complexes are convenient starting materials for metathesis, as the Mo–Br bonds are relatively labile, presumably a result of the steric effect of the larger Br ligand atom. Indeed, the lability of the Mo–Br bond of L^aMoO_2Br permits the formation of species such as $[L^aMoO_2(solv)]^+$ or $L^aMoO_2(OH)$ with subsequent condensation to $[L^aMo^{VI}O_2]_2(\mu\text{-}O)$.[30] Mononuclear L^aMoO_2Br may be separated from the dinuclear complex by chromatography for use in metathesis reactions. Synthesis of the bromo complex of the bulkier L^b ligand is not complicated by dinucleation. We have not identified $[L^cMoO_2]_2(\mu\text{-}O)$ in reactions to date.

The original synthesis of $L^aMoO_2(OMe)$ involved reaction of L^aMoO_2Br and MeOH/Et_3N in toluene at 60 °C for 4 h for a 48% yield.[10] Optimized conditions, viz., reaction of L^aMoO_2Br and MeOH/NaOH in CH_2Cl_2 at 40–50 °C, provide a greater than 80% yield in 10 min:

$$L^aMoO_2Br + MeOH + NaOH \rightarrow L^aMoO_2(OMe) + H_2O + NaBr \quad (2)$$

The approach is readily extended to other alkoxo derivatives, but the reaction times increase with the number of carbon atoms. The equivalent complexes for L^b are readily obtained at room temperature. The more basic character of L^c means that $L^cMoO_2(OMe)$ can be prepared in quantitative yield from L^cMoO_2Br and MeOH at room temperature. In fact, other L^cMoO_2X complexes are converted to $L^cMoO_2(OMe)$ in the presence of methanol:

$$L^cMoO_2X + MeOH \rightarrow L^cMoO_2(OMe) + HX \quad (3)$$

At room temperature in methanol, $L^cMoO_2(SPh)$ is converted quantitatively to $L^cMoO_2(OMe)$ in *ca.* 5 h; for $L^cMoO_2(OPh)$, such conversion is complete overnight. By contrast, L^aMoO_2X and L^bMoO_2X are stable under the same conditions, and methanol is a convenient solvent for isolation and crystallization of these complexes. Other complexes $L^cMoO_2(ER)$ (E = O, S; R = alkyl, phenyl) were all prepared readily in high yield by metathesis of L^cMoO_2Br with the appropriate ROH or RSH in CH_2Cl_2 under basic conditions. The reactions all proceed smoothly at room temperature, and no heating is required. However, heating is necessary to obtain L^a complexes such as $L^aMoO_2(OPh)$ and $L^aMoO_2(SPr^i)$.

A significant advantage in the synthesis of $LMoO_2(SR)$ complexes is gained through the use of RSH/NEt_3 rather than NaSR as the source of SR^- and more importantly by carrying out the reaction in chlorinated solvents rather than in toluene. This increases the solubility of the reactants, avoids the reduction of starting material through undue heating, and permits the synthesis of $L^aMoO_2(SPh)$, the cornerstone of a recent molybdoenzyme model,[11] in >90% yield (cf. 14% using NaSPh/toluene at 70 °C[10]).

Microanalytical and spectroscopic data are consistent with the proposed formulations. Infrared spectra (Table 1) are consistent with the presence of a $[MoO_2]^{2+}$ unit and the various coligands. The presence of a single broad ν(CN) band in the

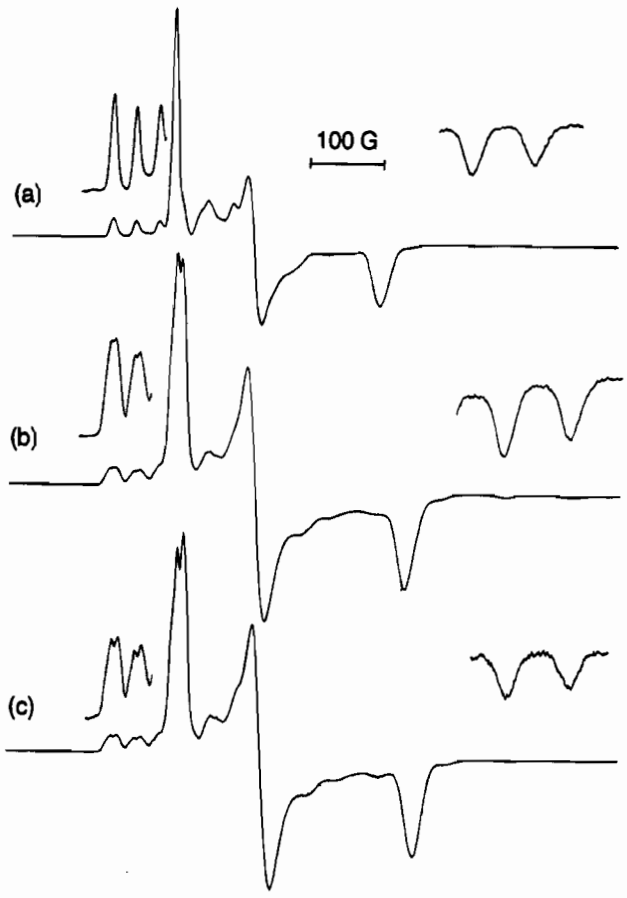

Figure 9. EPR spectra at 77 K generated by the reduction of $LMoO_2Cl$ by a 7-fold excess of Bu^n_4NSH in THF/MeCN (10/1), showing $^{35,37}Cl$ coupling in one direction: (a) L^a; (b) L^b; (c) L^c.

(44) The carbonyl–Mo(0) complex $NEt_4[L^cMo(CO)_3]$ exhibits ν(CO) bands at 1900 and 1765 cm^{-1} while the L^a analogue exhibits bands at 1890 and 1750 cm^{-1}. This is consistent with less π-back-bonding in the L^c complex, a consequence of the electron-withdrawing nature of L^c: Macleod, I. T.; Tiekink, E. R. T.; Young, C. G. *J. Organomet. Chem.*, in press.

L^b complexes is notable as it is diagnostic of the hydrotris(3-isopropylpyrazol-1-yl)borate ligand.[40] The high frequencies of the $\nu(MoO_2)$ modes of L^cMoO_2X relative to those of L^aMoO_2X are consistent with the greater electron-withdrawing capacity of L^c relative to L^a.[44] The ^1H NMR spectra of the complexes (Table 2) are indicative of molecular C_s symmetry in solution. For the L^aMoO_2X complexes, the chemical shift of the unique methine proton is very similar to or greater than that of the other two methine protons, a feature diagnostic of L^aMO_2X (M = Mo,[10] W[45]) complexes. For the L^bMoO_2X complexes, the methyl groups of two of the isopropyl groups are diastereotopic, whereas those of the unique isopropyl group are enantiotopic. This leads to three pairs of symmetry-related methyl groups in all complexes; coupling to the methine hydrogens produces three doublet resonances. The spectra also support the presence of the hydrotris(3-isopropylpyrazol-1-yl)borate ligand in the solution species.[40] The conclusion drawn from comparative IR and NMR studies was confirmed by the X-ray structure of $L^bMoO_2(OMe)$. The deshielding of the methyl resonances of the L^cMoO_2X complexes relative to the L^aMoO_2X analogues is consistent with the presence of the electronegative ring nitrogen in L^c.

The structures determined for $L^aMoO_2(SPh)$, $L^bMoO_2(OMe)$, and $L^cMoO_2(SPh)$ are in accord with expectations. The structural parameters of the $[Mo^{VI}O_2]^{2+}$ fragment in each complex are identical within experiment error (Table 7). They are typical of other such species and are virtually identical to those observed in $L^aMoO_2(NCS)$[10] and $L^aMoO_2\{S_2P(OEt)_2\}$.[9] Repulsions between the π-electrons in the Mo=O bonds account for an O−Mo−O bond angle greater than the octahedral angle of 90°.[46] The Mo−S distances (average 2.40 Å) are slightly longer than the Mo−S distances in $L^aMo^VO(SPh)_2$ (average 2.382 Å[12]) or $L^aMo^{IV}O$(pyridine)(SPh) (2.390 Å[47]). The Mo−S−C(1) angles (average 105.7°) are less obtuse than the Mo−S−C angles in the latter two complexes (115.1 and 115.6°, respectively). The lack of a second oxo ligand in the $Mo^{IV,V}$ species may strengthen the Mo−SPh π interaction and increase the Mo−S−C angle. The oxo ligands, as expected, exert a strong *trans* effect on the Mo−N(21) and Mo−N(31) bonds, lengthening them significantly with respect to the Mo−N(11) bond. The arrangement of the SPh^- groups provides maximum steric protection for the $[Mo^{VI}O_2]^{2+}$ fragment and prevents dinucleation upon reduction. The Mo−O(3) bond of L^bMoO_2(OMe) (1.865(2) Å) is much longer than the Mo=O bonds, consistent with a single-bond representation. The significant lengthening of the Mo−N bonds of $L^bMoO_2(OMe)$ compared to $L^aMoO_2(SPh)$ may be reasonably ascribed to the presence of the bulkier 3-isopropyl groups in L^b. The L^bMoO_2X complexes are less stable in solution than their L^a counterparts and decompose gradually in $CHCl_3$, releasing free L^b ligand, as monitored by ^1H NMR spectroscopy. This may be related to steric congestion and the longer Mo−N bonds. The Mo=O distances in $L^cMoO_2(SPh)$ are significantly shorter than those of the Mo(V) anion $[L^cMoO_2(SPh)]^-$ [1.742(9) Å], and the O=Mo=O angle is smaller than that of the anion [112.1(4)°].[20] These observations are consistent with the absence of a metal-based but sterically consequential d^1 electron in the Mo(VI) complex.

The redox behavior of dioxo−Mo(VI) complexes is of crucial importance in developing models for the pterin-containing molybdenum enzymes, which shuttle between the Mo(VI), Mo(V), and Mo(IV) oxidation levels during turnover.[3-5] Almost all dioxo−Mo(VI) complexes exhibit irreversible electrochemical behavior and produce $[Mo^VO]^{3+}$, $[Mo^V_2O_3]^{4+}$, or $[Mo^{IV}O]^{2+}$ species upon reduction.[3,4] This appears to result from (a) inadequate steric inhibition of dinucleation of initially formed *cis*-$[Mo^VO_2]^+$ or *cis*-$[Mo^VO(OH)]^{2+}$ centers and (b) the ability of ligands to accommodate stereochemical changes which enhance the rate of dinucleation, e.g. *cis*-$[MoO(OH)]^{2+}$ to *trans*-$[MoO(OH)]^{2+}$. The hydroxo ligands may be eliminated either as OH^- or as H_2O, depending on the availability of protons. This dimerization can be written as

$$2L_nMo^VO(OH) \rightarrow (L_n)_2Mo^V_2O_3 + H_2O \qquad (4)$$

Alternatively, conformational changes and/or loss of an oxo ligand can promote further reduction to Mo(IV) species, which may undergo comproportionation with the remaining dioxo−Mo(VI) complex to yield the same dinuclear species:

$$L_nMo^{VI}O_2 + L_nMo^{IV}O \rightarrow (L_n)_2Mo^V_2O_3 \qquad (5)$$

The rate of substitution is slower at sites *cis* to the oxo ligand in $[Mo^VO]^{3+}$ complexes than at sites *trans* to the oxo group. Moreover, in *cis*-$[Mo^VO(OH)]^{2+}$ complexes, the hydroxo ligand does not appear to protonate further and undergo elimination as water. The requirements for *reversible* one-electron electrochemical reduction of dioxo−Mo(VI) complexes appear to be (i) minimal conformational change, restricting substitution *trans* to the oxo groups, upon reduction and (ii) a steric or electrostatic barrier to the close approach and dinucleation of the reduced species.

With the exception of L^cMoO_2Cl, the $LMoO_2X$ (X = Cl, Br, SCN) complexes undergo irreversible electrochemical reduction. Although requirement i is enforced by the ligands L, it appears that requirement ii is not met by these complexes. This may be attributed to the hydrolysis of a labile Mo^V-X or Mo^V-OH bond upon reduction of these complexes and the inability of the L ligands to alone prevent dinucleation.[30] Interestingly, chemically generated $[L^cMoO_2X]^-$ complexes are not observed to protonate to form the corresponding oxo−hydroxo species. Thus, in the absence of elimination of X^-, electrostatic repulsion may effectively counter the close approach necessary for dinucleation and lead to reversible electrochemistry. The greater electron-withdrawing ability of L^c accounts for the stability and relatively low basicity of the $[L^cMoO_2X]^-$ complexes.

In contrast, the $LMoO_2X$ (X = OR, SR) complexes undergo an electrochemically reversible one-electron reduction process (eq 6; Table 8). They constitute the first extended series of

$$LMo^{VI}O_2X + e^- \rightarrow [LMo^VO_2X]^- \qquad (6)$$

dioxo−Mo(VI) complexes to exhibit this property; both requirements i and ii would appear to be met. The reversibility of the process permits examination of the influence of the ligands L and X upon the reduction potentials. This is important since the reduction potentials of dioxo−Mo(VI) complexes are related directly to their oxygen atom transfer activities.[48] Both processes involve donation of electron(s) into a π^* (principally metal-based) LUMO of the $[Mo^{VI}O_2]^{2+}$ fragment.

The measured $E_{1/2}$ values depend upon L, such that $E_{1/2}(L^cMoO_2X) > E_{1/2}(L^bMoO_2X) > E_{1/2}(L^aMoO_2X)$ for a given ligand X (Table 8). Thus, $E_{1/2}$ for the predominantly metal-centered reduction is sensitive to the type and substitution pattern

(45) Eagle A. A.; Young, C. G.; Tiekink, E. R. T. *Organometallics* **1992**, *11*, 2934.
(46) Cotton, F. A.; Morehouse, S. M. *Inorg. Chem.* **1965**, *4*, 1377.
(47) Xiao, Z.; Bruck, M.; Enemark, J. H.; Young, C. G.; Wedd, A. G. Manuscript in preparation.
(48) Holm, R. H.; Donahue, J. P. *Polyhedron* **1993**, *12*, 571.

of the heterocyclic rings of L. Available data support the view that L^c is electron-withdrawing relative to L^a. Therefore, in L^c complexes, the Mo center will be more positive and the metal-based LUMO orbital lower in energy than in analogous L^a complexes. The more positive reduction potentials of L^cMoO_2X complexes compared to L^aMoO_2X species are consistent with this reasoning. The reduction potentials of the L^bMoO_2X complexes are also more positive than those of the corresponding L^aMoO_2X complexes because the L^a ligand is relatively electron-donating compared to the monosubstituted and bulkier L^b ligand. Spectroscopic ($\nu(MoO_2)$ and δ trends), structural, and electrochemical findings support the following relative ordering of ligands L according to electron-donating ability: $L^c < L^b < L^a$.

The influence of each X on $E_{1/2}$ is qualitatively the same between series with different ligands L: $LMoO_2(SR)$ complexes are easier to reduce than the $LMoO_2(OR)$ complexes, and the $LMoO_2(EPh)$ species are easier to reduce than $LMoO_2(ER)$ (E = O, S) complexes. These findings are consistent with the greater π-accepting ability of S over O and phenyl over alkyl. Therefore, reduction potentials of dioxo−Mo(VI) complexes are not only sensitive to the nature of the donor atoms but also sensitive to remote changes in the ligands. These effects are also observed in oxo−Mo(V) complexes.[12,14]

Reduction of $LMo^{VI}O_2X$ results in EPR-active Mo(V) species. The isotropic and anisotropic g values and the isotropic ^{95,97}Mo hyperfine parameters, A, for each complex are listed in Tables 10−12. The reversible nature of the reduction and the EPR activity of the products confirm the production of mononuclear species, while a detailed analysis of the EPR spectra, especially a comparison with previously reported results,[22−24] permits confident structural assignments to be made. In each case, the initial product of reduction is the dioxo−Mo(V) anion $[LMoO_2X]^-$; these are characterized by highly anisotropic frozen-glass EPR spectra and very low g values. The width of the central $I = 0$ component of the solution spectra (Figure 7a), a characteristic of such complexes, is due to incomplete motional averaging of the highly anisotropic **g** tensor with its very low g_3.[22] The variation in line width across the ^{95,97}Mo hyperfine sextet is due to an additional dependence of line width upon magnetic quantum number m_I.[49] These species may be generated chemically by reduction of $LMoO_2X$ with Bu^n_4NSH in THF and can only exist in carefully dried aprotic solvents or in basic conditions such as Bu^n_4NSH solution. This interpretation is confirmed by the isolation and full characterization of $[CoCp_2][LMo^VO_2(SPh)]$ complexes, obtained by cobaltocene reduction of $LMoO_2(SPh)$ in MeCN.[11,20,42] The EPR parameters of these complexes are similar to those of $[(L\text{-}N_2S_2)MoO_2]^-$;[22−24] the EPR spectrum of this complex has been simulated successfully assuming C_{2v} local symmetry (i.e., two equivalent oxo ligands) and a d_{xy} magnetic orbital (z axis bisects the O−Mo−O angle). The demand for facial coordination by the tridentate ligand L requires the two oxo ligands to be *cis* in $[LMoO_2X]^-$. Hence, such complexes should possess the same local C_s symmetry as $LMoO_2X$, with either a d_{yz} or d_{xy} magnetic orbital (with x perpendicular to the mirror plane and z bisecting the O−Mo−O angle; see Figure 10a). This is supported by the EPR spectrum of $[LMoO_2Cl]^-$ (Figure 9). Coupling to the chlorine nucleus is anisotropic with the largest component in one direction. This is consistent with a strong π interaction between Mo d_{yz} and Cl p_z or Mo d_{xy} and Cl p_x orbitals (Figure 10a). A stronger electron-withdrawing ligand should lower the energy of the metal-based LUMO and enhance such interactions. Thus the magnitude of the coupling increases in concert with the electron-withdrawing power of L, viz. $[L^cMoO_2Cl]^- > [L^bMoO_2Cl]^- > [L^aMoO_2Cl]^-$ (Figure 9). The coupling is essentially not detectable in $[L^aMoO_2Cl]^-$.

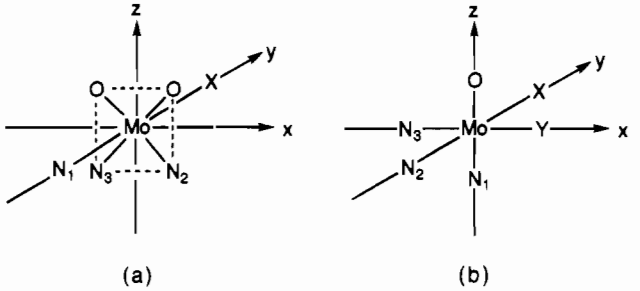

Figure 10. Coordinate systems for (a) $[LMoO_2X]^-$ and (b) $[LMoOYX]^{n-}$ (Y = OH, $n = 0$; Y = S, $n = 1$).

In wet solvents, the dioxo−Mo(V) anions of L^a and L^b protonate rapidly by reaction with trace water, producing the conjugate acids $LMo^VO(OH)X$. Their EPR spectra exhibit superhyperfine coupling to a single proton. One of the oxo groups is converted to a hydroxo ligand, and the symmetry is lowered from C_s in $[LMoO_2X]^-$ to C_1 in LMoO(OH)X (Figure 10b). The oxo ligand is expected to dominate the ligand field, and the observed parameters are consistent with a d_{xy} magnetic orbital (z axis along the Mo=O bond).[50] Both the EPR spectra in liquid solution and in frozen solution are split by strong coupling to the hydroxo proton. The coupling constants $A(^1H)$ range from 9.6 to 14 × 10^{-4} cm^{-1}, comparable with those for the enzymes[51,52] as well as other model systems.[22,23] This is again consistent with a *cis*-$[Mo^VO(OH)]^{2+}$ species. As observed previously,[12,14] the complexes with sulfur donor atoms have a higher g value and lower A value than corresponding oxygen atom donor complexes.

Hydrosulfide reduces the $LMoO_2X$ complexes to the corresponding anions $[LMoO_2X]^-$. While a clean reaction does not take place when X = OR (R = alkyl), the other complexes are reduced rapidly to green Mo(V) complexes. For X = Cl, Br, NCS, and SCH_2Ph, the initial signal for $[LMoO_2X]^-$ is replaced after several hours by signals ascribed to $[LMoOSX]^-$ (see Figure 8), indicating a slow substitution of oxo by thio

$$[LMoO_2X]^- + SH^- \rightarrow [LMoOSX]^- + OH^- \qquad (7)$$

Assignment of the new signals to $[LMoOSX]^-$ complexes is supported by variation of their EPR parameters with different X and by their close EPR spectral similarities to $[(L\text{-}N_2S_2)MoOS]^-$ (Table 12).[22,23] Notably, thio substitution results in an increase of all three anisotropic g values, particularly g_1 > $g_e = 2.0023$, and therefore of g, but leads to a decrease in A. Substitution of thio for oxo in $L^aMo^VOCl_2$ to give $L^aMo^VSCl_2$ has been found to lower g from 1.947 to 1.928 but has little effect on A.[13] The observations are consistent with a bonding scheme derived for $[(L\text{-}N_2S_2)MoOS]^-$ (Figure 10b):[23] the oxo ligand dominates the ligand field, forcing the magnetic orbital into the xy plane; the Mo−thio link features a $Mo(d_{xy})-S(p_y)$ π interaction, but the formal bond order is 1.5 due to the occupation of a highly delocalized π^* orbital by the magnetic electron.[23] Coupling to the Cl nucleus is observed for $[L^bMoO_2Cl]^-$ but is not observed for $[L^bMoOSCl]^-$, consistent with reduced coupling due to a stronger Mo d_{xy} and S p_y π interaction.

(49) Hanson, G. R.; Brunette, A. A.; McDonell, A. C.; Murray, K. S.; Wedd, A. G. *J. Am. Chem. Soc.* **1981**, *103*, 1953.

(50) Carducci, M. D.; Brown, C.; Solomon, E. I.; Enemark, J. H. *J. Am. Chem. Soc.* **1994**, *116*, 11856.

(51) Bray, R. C. *Adv. Enzymol. Relat. Areas Mol. Biol.* **1980**, *51*, 107.

For X = OPh, SPh, and SPr^i, the green solution is stable and exhibits a strong EPR signal characteristic of anionic species $[LMoO_2X]^-$. This demonstrates that reaction 7 is critically dependent on the steric properties of X.

Interestingly, only when dioxo−Mo(VI) complexes have been reduced to dioxo−Mo(V) species, can the oxo−thio substitution be effected, consistent with a weakening of the oxo−Mo bonds upon reduction. No such substitution is observed between $LMo^{VI}O_2(OR)$ (R = Me, Et) and Bu^n_4NSH, presumably because of the inability of SH^- to reduce these complexes. In addition, the complexes $LMoO_2X$ do not undergo oxygen atom exchange with water while $L^{a,b}MoO(OH)X$ [and by inference $L^cMoO(OH)X$] can complete such an exchange in several hours:[42]

$$L^{a,b}MoO(OH)X + 2H_2{}^*O \rightarrow L^{a,b}Mo{}^*O({}^*OH)X + 2H_2O \quad (8)$$

It is surprising that the complexes $[LMoO_2(EPh)]^-$ (E = O, S) and $[L^aMoO_2(SPr^i)]^-$ do not undergo oxo−thio substitution but that $L^aMoO(OH)(SPh)$ and $L^bMoO(OH)(SPh)$ do undergo oxygen atom exchange with water. It is possible that the steric bulk of the EPh^- ligand prevents access of SH^-, but not smaller OH_2, to the Mo(V) center.

Attempts to isolate anionic species $[L^aMoOSX]^-$ were unsuccessful. These species are not stable in solution and, under the conditions explored here, decompose slowly to yield $(Bu^n_4N)_2[MoOS_3]$. Attempts to oxidize $[L^aMoOSX]^-$ to L^a-MoOSX in solution by introducing dioxygen resulted in the isolation of the binuclear complex $[L^aMo^VO]_2(\mu\text{-}O)(\mu\text{-}S_2)$ as a major product.[30,53]

Conclusion

This work reports efficient synthetic methods and the detailed characterization of an extended series of dioxo−Mo(VI) complexes of the type $LMoO_2X$, where L is a tripodal monoanionic N-donor ligand. Variation in the tripodal and monodentate ligands permits steric and electronic fine-tuning of the properties of the $[MoO_2]^{2+}$ core and enables the one-electron reduction and coupled electron−proton transfer reactions of this biologically important center[2-5] to be systematically investigated. Mononuclear oxo−Mo(V) species, such as $[LMo^VO_2X]^-$, $LMo^VO(OH)X$, and $[LMo^VOSX]^-$, have been generated in solution and studied by EPR spectroscopy. For $X = RS^-$, the Mo(VI/V) couple is electrochemically reversible, and all three of the above Mo(V) centers are accessible in this case. The ability to study $[LMo^VOSX]^-$ complexes with a wide range of X groups has revealed that g_1 is greater than 2.0023 for all X ligands. Thus, for these complexes, the $[MoOS]^+$ unit dominates the electronic structure as proposed from previous studies of $[(L\text{-}N_2S_2)Mo^VOS]^-$,[22-24] and the presence of additional sulfur ligands has relatively little effect on the observed EPR parameters.

Finally, catalysis by pterin-containing molybdenum enzymes may involve oxygen atom transfer and/or coupled electron−proton processes.[2-5] Oxygen atom transfer chemistry has been extensively reviewed[18] and demonstrated by isotopic labeling for model compounds and enzymes,[54-56] but coupled electron−proton reactions have not been as extensively studied.[3,4] The $LMoO_2X$ compounds investigated here exhibit both atom transfer and coupled electron−proton chemistry[11] that can be modulated by varying L and X. As such, these compounds continue to provide a fascinating window on the chemical tranformations and spectroscopic properties of oxo−molybdenum centers.

Acknowledgment. Z.X. thanks La Trobe University for the award of a postgraduate scholarship. We gratefully acknowledge the financial support of the Australian Research Council and the National Institutes of Health (Grant GM-37773 to J.H.E.).

Supporting Information Available: Tables of crystallographic data, positional and thermal parameters, and bond distances and angles for $L^aMoO_2(SPh)$, $L^bMoO_2(OMe)$, and $L^cMoO_2(SPh)$ (20 pages). Ordering information is given on any current masthead page.

IC950398D

(52) Bray, R. C. *Q. Rev. Biophys.* **1988**, *21*, 299.

(53) Related oxo−thio−Mo(V) complexes such as $[L^aMoOS\{SP(S)Pr^i_2\}]^-$ are oxidized to oxo−thio−Mo(VI) complexes by dioxygen. In these complexes, stabilization of the nascent thio−Mo(VI) moiety by an intramolecular sulfur−sulfur interaction is possible: Laughlin, L. J.; Young, C. G. *Inorg. Chem.*, in press. See also ref 21.

(54) Hille, R.; Sprecher, H. *J. Biol. Chem.* **1987**, *262*, 10914.

(55) Schultz, B. E.; Gheller, S. F.; Muetterties, M. C.; Scott, M. J.; Holm, R. H. *J. Am. Chem. Soc.* **1993**, *115*, 2714.

(56) Schultz, B. E.; Hille, R.; Holm, R. H. *J. Am. Chem. Soc.* **1995**, *117*, 827.